Democratic and Popular Republic of Algeria

Ministry of Higher Education and Scientific Research

Larbi Tebessi University

Faculty of Exact Sciences and Sciences of Life and Nature

Department of Matter Sciences

MASTER'S THESIS

Field: Matter Sciences

Discipline: Physics

Option: Condensed Matter Physics

Theme:

Study of the spectroscopic properties of ^{26}Al and ^{27}Al

Presented by:

ZIANI ABLA *AIDOUDI KHAOULA*

Board of Examiners:

Chair:	CHEMAM Faïçal	**Professor**	Larbi Tebessi University
Supervisor:	BOUHELAL Mouna	**Professor**	Larbi Tebessi University
Examiner:	SERDOUK Fadhila	**MCB**	Larbi Tebessi University

***Date of defence*: 21/06/2022**

Note: …… **Mention: …**

Université Larbi Tebessi- Tébessa

Faculté des sciences exactes et des sciences de la nature et de la vie

Département Sciences de la matière

Filière : Physique

Spécialité : Physique de la matière condensée

Année universitaire : 2021/2022

Formulaire de levée de réserves après soutenance d'un Mémoire de Master

Données d'identification du candidats (es) :

Nom et prénom du candidat : ZIANI Abla & Aidoudi Khaoula

Intitulé du Sujet : ***Study of the spectroscopic proprietes of the 26 AL and 27 AL***

Données d'identification du membre de jury :

Nom et prénom : CHEMAM Faiçal

Grade : Prof

Lieu d'exercice : Université Larbi Tebessi – Tébessa-

Vu le procès-verbal de soutenance de la thèse sus citée comportant les réserves suivantes :

.....

.....

RAS

.....

.....

Et après constatation des modifications et corrections suivantes :

.....

.....

RAS

.....

.....

Je déclare en ma qualité de président de jury de soutenance que le mémoire cité remplit toutes les conditions exigées et permet au candidat de déposer son mémoire en vue de l'obtention de l'attestation de succès.

Le :

Président de jury de soutenance : (Nom/Prénom et signature)

le 07/07/2022

Prof. CHEMAM Faiçal

Université Larbi Tébessi- Tébessa
Faculté des sciences exactes et des sciences de la nature et de la vie
Département de ..Science de la matière
Filière : ..Physique..
Année universitaire 2021/2022

Déclaration sur l'honneur de non-plagiat
(A joindre obligatoirement avec le mémoire)

Je, soussigné(e)
Nom et prénom : Ziani Abla
Régulièrement inscrit (e) : Master 2
N de carte d'étudiant : 151534029406
Année universitaire : 2021/2022
Domaine : Science de la matière
Filière : Physique
Spécialité : Physique de la matière condensé
Intitulé :

Atteste que mon mémoire est un travail original et que toutes les sources utilisées ont été indiquées dans leur totalité, je certifie également que je n'ai ni copié ni utilisé des idées ou des formulations tirées d'un ouvrage, article ou mémoire, en version imprimée ou électronique, sans mentionner précisément leur origine et que les citations intégrales sont signalées entre guillemets.

Sanctions en cas de plagiat prouvé :

L'étudiant sera convoqué devant le conseil de discipline, les sanctions prévues selon la gravité de plagiat sont :

- L'annulation du mémoire avec possibilité de refaire sur un sujet différent.
- L'exclusion d'une année de Master.
- L'exclusion définitive.

Fait à Tébessa, le :
Signature de l'étudiant (e)

Université Larbi Tébessi- Tébessa

Faculté des sciences exactes et des sciences de la nature et de la vie

Département de Science de la matière

Filière : Physique

Année universitaire 2021/2022

Déclaration sur l'honneur de non-plagiat (A joindre obligatoirement avec le mémoire)

Je, soussigné(e)

Nom et prénom : Aidoudi Khaoula

Régulièrement inscrit (e) : Master 02

N de carte d'étudiant : 115340276 25

Année universitaire : 2021/2022

Domaine : Science de la matière

Filière : physique

Spécialité : physique de la matière condensée

Intitulé :

Atteste que mon mémoire est un travail original et que toutes les sources utilisées ont été indiquées dans leur totalité, je certifie également que je n'ai ni copié ni utilisé des idées ou des formulations tirées d'un ouvrage, article ou mémoire, en version imprimée ou électronique, sans mentionner précisément leur origine et que les citations intégrales sont signalées entre guillemets.

Sanctions en cas de plagiat prouvé :

L'étudiant sera convoqué devant le conseil de discipline, les sanctions prévues selon la gravité de plagiat sont :

- *L'annulation du mémoire avec possibilité de refaire sur un sujet différent.*
- *L'exclusion d'une année de Master.*
- *L'exclusion définitive.*

Fait à Tébessa, le :

Signature de l'étudiant (e)

Thesis achieved at

Laboratoire de Physique Appliquée et Théorique LPAT

Abstract

Abstract

The nuclear shell model is one of the most important models describing the structure of the nucleus in terms of energy spectra and electromagnetic properties.

Nuclei in the **sd** region are a good test for many basic models, such as shell model. These nuclei are characterized by the coexistence, at low excitation energies, of normal positive- and intruder negative- parity states. The description of normal positive parity states has been done using the well-known **USD** or **USDA/B** effective interactions. The **PSDPF** interaction describes, in a consistent way, the normal positive- and intruder negative- parity states.

The main aim of this work is the use of the **PSDPF** interaction to describe the complete energy spectra of both positive- and negative- parity states of ^{26}**Al** and ^{27}**Al**, and then compared them to available experimental data. The calculation of the electromagnetic transitions of the first excited states has been also carried out. The obtained results are in good agreement with experiment, up to high excitation energies.

ملخص

ملخص

نموذج الطبقات النووي هو واحد من أهم النماذج الواصفة لبنية النواة فيما يخص أطياف الطاقة والخصائص الكهرومغناطيسية.

أنوية الطبقة **sd** هي اختبارا جيدا للعديد من النماذج الأساسية، مثل نموذج الطبقات. تتميز هذه الأنوية بحالات ذات زوجية موجبة وسالبة عند طاقات الاثارة المنخفضة. تم وصف الحالات ذات الزوجية الموجبة باستخدام التفاعلات الفعالة المعرفة جيدا **USD** او **USDA/B**. التفاعل **PSDPF** يصف، بطريقة متسقة، الحالات العادية ذات الزوجية الموجبة و الدخيلة ذات الزوجية السالبة.

الهدف الرئيسي من هذا العمل هو استخدام التفاعل **PSDPF** لوصف اطياف الطاقة الكاملة لكل من حالات التكافؤ الإيجابية والسلبية للنظيرين ^{26}Al و^{27}Al ثم مقارنتها بالبيانات التجريبية المتاحة. أيضا تم حساب الانتقالات الكهرومغناطيسية للحالات المثارة الأولى. النتائج التي تم الحصول عليها تتفق بشكل جيد مع التجربة و ذلك حتى طاقات الاثارة العالية.

Résumé

Résumé

Le modèle en couches nucléaire est l'un des modèles les plus importants décrivant la structure du noyau en termes des spectres énergétiques et des propriétés électromagnétiques.

Les noyaux de la région sd sont un bon test pour de nombreux modèles de base, tels que le modèle en couches. Ces noyaux sont caractérisés par la coexistence, à faibles énergies d'excitation, d'états normaux de parité positive et intrus de parité négative. La description des états normaux de parité positive a été faite en utilisant les interactions effectives bien connues **USD** ou **USDA/B**. L'interaction PSDPF décrit, de manière cohérente, les états normaux de parité positive et intrus de parité négative.

L'objectif principal de ce travail est l'utilisation de l'interaction **PSDPF** pour décrire les spectres en énergie complets des états de parité- positive et négative de ^{26}Al et ^{27}Al, puis de les comparer aux données expérimentales disponibles. Le calcul des transitions électromagnétiques des premiers états excités a également été effectué. Les résultats obtenus sont en bon accord avec l'expérience jusqu'aux hautes énergies d'excitation.

Acknowledgements

*Firstly, we would like to thank specially our supervisor **Professor BOUHELAL Mouna** who made this work possible, for providing her invaluable guidance, her support, understanding and advices, thank you so much.*

*We would like to acknowledge our committee members **Professor CHEMAM Faïçal** for chairing our thesis and **Doctor SERDOUK Fadhila** for examining our work. Thank you for joining our committee.*

*We would also like to acknowledge the **PHD** Student **SELIM Abir** for co-supervising our thesis, for giving us a helping hand when we asked for it, thanks for you.*

*We extend our thanks to our distinguished professors and to all those who have helped us in our journey. We would thank all the employees of the Department specially **Mr ACHOUR Khelifa** and **Ms GUOUASSMIAHanene**.*

Abla's Dedication

First of all, Alhamdoulilah for the the blessing, and thanks to Allah who enabled me to complete my work.

Thanks to myself that never gave up.

I dedicate this work to the two dearest persons in my life; my parents ***"SAID"*** *and* ***"NADJETTE"*** *who waited for this day to see me as a successful person, you are my life.*

To my only soul, my brother ***"ANTAR",*** *may ALLAH protect you, I'm proud that you are my brother.*

To my beloved sisters ***"AZIZA"*** *and* ***"HIBA",*** *thanks for being with me.*

*To my life partner, my husband "****SAID BOUTOUBA****", you are my support and the first one who encouraged me, thank you so much for everything. I'm glad to have you.*

To my family ***"ZIANI ",*** *my grandfathers and grandmothers, all my uncles and aunts, and my cousins for their support.*

Thanks to everyone who taught me a letter.

ZIANI ABLA

Khaoula's Dedication

In the name of ALLAH the Merciful

First of all, thanks ALLAH,

I dedicate this humble work to my parents to

*my father "**Elfateh**", keep your head up your daughter finally did it*

my wonderful mother for her measureless support, encouragement, and her constant love

my brothers and friends who supported me and helped me in completing my thesis

To all who knew me and to all those who did not know me yet, I dedicate this humble work to you.

To every person has supported me in my journey.

AIDOUDI KHAOULA

Table of Contents

List of Tables

List of Figures

List of Symbols

Z	Number of protons
N	Number of neutrons
A	Atomic number
$\mathbf{V_{OH}}$	Harmonic-oscillator potential
$\mathbf{H_0}$	The independent movement of nucleons in the nucleus
Ω	The harmonic-Oscillator frequency
$\mathbf{h_i}$	The Hamiltonian of an individual nucleon
$\mathbf{V_{ij}}$	Two-body interaction between the nucleons i and j
$\mathbf{H_r}$	The residual interaction.
$\boldsymbol{E_i}$	Initial state energy
$\boldsymbol{E_f}$	Final state energy
μ_N	The nuclear magneton
$\boldsymbol{\Gamma_\gamma}$	The transition widths
$\boldsymbol{\Gamma_w}$	Weisskopf estimation
$\boldsymbol{\tau_m}$	The mean life time
$\boldsymbol{Y_{LM}}$	Spherical harmonic
EL	Electric transition
ML	Magnetic transition
e(k)	The nucleon k effective charge
ΔE	The difference in energy
$\boldsymbol{g^l, g^s}$	Gyromagnetic factors of orbit and spin, respectively
$\boldsymbol{T_{1/2}}$	Half-life
USD	sd-shell universal interaction compatible with sd valence space
USDA	sd-shell universal interaction compatible with sd valence space (updated version of the USD interaction)
USDB	sd-shell universal interaction compatible with sd valence space (updated version of the USD interaction)
PDSPF	Effective interaction for sd-shell nuclei compatible with p-sd-pf valence space
0ħω	(0 particle-0 hole jump) denotes the positive parity states
1ħω	(1 particle-1 hole jump) denotes the negative parity states

Introduction

Introduction

The nuclear shell model was the most successful theoretical nuclear model, which describes the way protons and neutrons are arranged (structure) inside a nucleus. The obtained structure have been well reproduced using simple shell-model wave functions and effective two-body interactions. Application of the shell model to the study of various regions of nuclei has led to the determination of many nuclear properties (energy spectra, electromagnetic transitions, angular momenta, magnetic moments, etc.).

The **sd** shell nuclei region is located between the two doubly-magic nuclei ^{16}**O** and ^{40}**Ca**, which have a number of neutrons **N** and protons **Z** between 8 and 20. The experimental spectra of these nuclei are characterized by the coexistence of normal positive parity states (**0ħω** states) and of intruder negative parity states (**1ħω** states). The shell model using the **USD** or **USDA/B** interactions, whose matrix elements were extracted from experimental data in a consistent way, describes successfully the **0ħω** states. In order to produce the two previous kinds of states (+ and -), the **PSDPF** interaction has been developed using a fitting procedure. This interaction describes quite well the intruder states of nuclei at the beginning of the **sd** shell around ^{16}**O** (resulting from p-**sd** jump) and at the end of the **sd** shell near ^{40}**Ca** (resulting from sd-pf jump). Note that in this fitting procedure, only the **1ħω** states of nuclei at the beginning ($^{16\text{-}20}$**O,** $^{18\text{-}21}$**F**, $^{20\text{-}22}$**Ne**), and at the end (^{33,34}**Si,** ^{34,35}**P,** ^{35,36}**S,** $^{35\text{-}37}$**Cl,** $^{36\text{-}38}$**Ar,** ^{38,39}**K,** ^{40}**Ca**) have been included. Concerning nuclei at the middle of **sd** shell, it is found that the states may have a competition between the two **p–sd** and **sd–pf** excitations. These nuclei could not be included in the fit due to the limitation of computing power.

In order to deeply test **PSDPF** in these nuclei, we studied previously the Sulfur, Phosphorus, and Silicon isotopic chains. In our thesis, we are going to study the spectroscopic properties of both isotopes ^{26}**Al** and ^{27}**Al**.

This manuscript contains three fundamental chapters distributed as the following:

- **Chapter I:** presents the basic notions of the nuclear shell model.
- **Chapter II:** reminds a short review of the **sd** shell nuclei and of the PSDPF interaction.
- **Chapter III:** presents a study of ^{26}**Al** and ^{27}**Al** in which we will expose the discussion of spectroscopic properties results and their comparison to experimental available data.

Our thesis will end by a conclusion.

Chapter I

Chapter I

Nuclear shell model

The nuclear shell model was introduced to explain the regularities of nuclear properties associated with magic numbers. This model has had quantitative and qualitative progress for the understanding of the nuclear structure based on the elementary interaction between nucleons. This interaction or even the nuclear force is not known with precision, which leads to the use of effective interactions. The underlying picture in this model is that each nucleon moves in a mean potential, which is created by its interaction with all the **(A-1)** other nucleons in the nucleus and is identical for all nucleons. In addition to this mean potential, an extra two-body interaction should be added. The latter depends on a chosen valence space; such as the **PSDPF** that is an interaction compatible with the **p-sd-pf** valence space [1].

In this chapter, we will introduce the essential concepts of the nuclear shell model, and its basic formalism. At the end, we will give a simple overview about electromagnetic transitions and isospin.

I. Shell model

The shell model is one of the fundamental tools of nuclear physics, which is generally synonymous with the Independent Particle Model that assumes a nucleon in the nucleus moves in a single-particle potential which represents its average interaction with the other **(A-1)** nucleons [2].

The nuclear shell model was introduced in 1949 by Maria G. Mayer [3] and independently by Haxel, Jensen and Suess [4], by analogy with the atomic shell model, to explain the regularities of the nuclear proprieties related to **N** and **Z** magic numbers.

I.1. Magic numbers

The magic numbers, discovered by Maria Geopert Mayer [3] and Otto Haxel, J. Hans Jensen [4], are **2, 8, 20, 28, 50, 82 or 126** corresponding to the total numbers of protons **Z** and/ or neutrons **N**. Nuclei, which have **Z** or **N** equal to one of the magic numbers are called

"magic nuclei", those with magic **Z** and **N** are called "doubly magic nuclei", and are found to be particularly stable.

I.2. Independent particle model

The nuclear independent particle model assumes that the nucleons in the nucleus move independently in an average potential (mean field), as explained previously. This potential could be approximated by a central potential. One of the simplest choices for the central potential is the harmonic oscillator potential [2]. The aim of this approach is the reproduction of all the magic numbers corresponding to the full filling of the obtained individual orbits.

- ✓ **The Harmonic Oscillator Potential**

The harmonic oscillator potential can be written as:

$$V_{H\text{-}O} = \frac{1}{2} m\, \omega^2\, r^2 \qquad \textbf{(1)}$$

Where **m** is the nucleon mass, **ω** is the harmonic oscillator frequency, and **r** is the distance between nucleon and the origin.

The Schrödinger equation for **A** nucleons is written as follows:

$$H_0\, \emptyset = E_0\, \emptyset \qquad \textbf{(2)}$$

where the Hamiltonian of independent particle potential is given by:

$$H_0 = \sum_{i=1}^{A} (t_i + v_i) = \sum_{i=1}^{A} \left(\frac{P_i^2}{2m} + \frac{1}{2}\, m\, \omega^2 r_i^2 \right) = \sum_{i=1}^{A} hi \qquad \textbf{(3)}$$

The Eigen functions can be given as:

$$\emptyset_{nlm_l}(r) = R_{nl}(r) Y_l^{m_l}(\theta, \varphi) \qquad \textbf{(4)}$$

Here ***l*** and **m*l*** are the quantum numbers of angular momentum and its **oz** projection respectively, whereas **n** is the radial quantum number.

The corresponding eigenvalues is:

$$E_{nl} = \left(N + \frac{3}{2} \right) \hbar\omega \qquad \textbf{(5)}$$

N represent the major number of the harmonic oscillator potential given by **N=2(*l* -1) + *l***.

- This potential reproduced only the first three magic numbers **2, 8, 20**.

✓ **Edge-board effect**

An improvement was brought by introducing a term representing to the "edge-board effect" **D*l*² (D<0)** [2] to make nucleons at the potential edge more bound. This correction made it possible to remove the degeneracy in ***l*** of the solution of Harmonic Oscillator. The Hamiltonian becomes:

$$h_{i=}t_i + \frac{1}{2}m\,\omega^2\,r^2 + Dl_i^2 \qquad \textbf{(6)}$$

With: $E^i_{nlj} = \left(N + \frac{3}{2}\right)\hbar\,\omega + Dl(l+1)\hbar^2$ **(7)**

- However, here again we do not find the correct sequence of the magic numbers.

✓ **Spin-orbit interaction**

Maria Geopert Mayer and Jensen, suggested that there is an additional strong attractive "single-particle spin-orbit" term [3, 4] given by:

$$V_{s-o} = f(r)\vec{l_i}\vec{s_i} \qquad \textbf{(8)}$$

The Hamiltonian of a single-particle becomes:

$$h_{i=}\,t_i + \frac{1}{2}m\,\omega^2 r_i^2 + Dl_i^2 + f(r)\vec{l_i}\,\vec{s_i} \qquad \textbf{(9)}$$

The obtained single-particle energies can be written as:

$$E_{nlj} = \left(N + \frac{3}{2}\right)\hbar\omega + Dl(l+1)\hbar^2 + \frac{\hbar^2}{2} < f(r) >_{nl} \begin{cases} -(l+1) & j = l - 1/2 \\ l & j = l + 1/2 \end{cases} \qquad \textbf{(10)}$$

The originally degenerate single-particle levels j=$\mathbf{l \pm 1/2}$ are split up.

The radial integral $< \boldsymbol{f(r)} >_{\boldsymbol{nl}}$ can be represented approximately by the relation:

$<f(r)>_{nl} \approx -20A^{-2/3}$ MeV [2],

which means that states with **j=l+1/2** are lower in energy than states with **j=l-1/2,** as shown on Figure I.1.

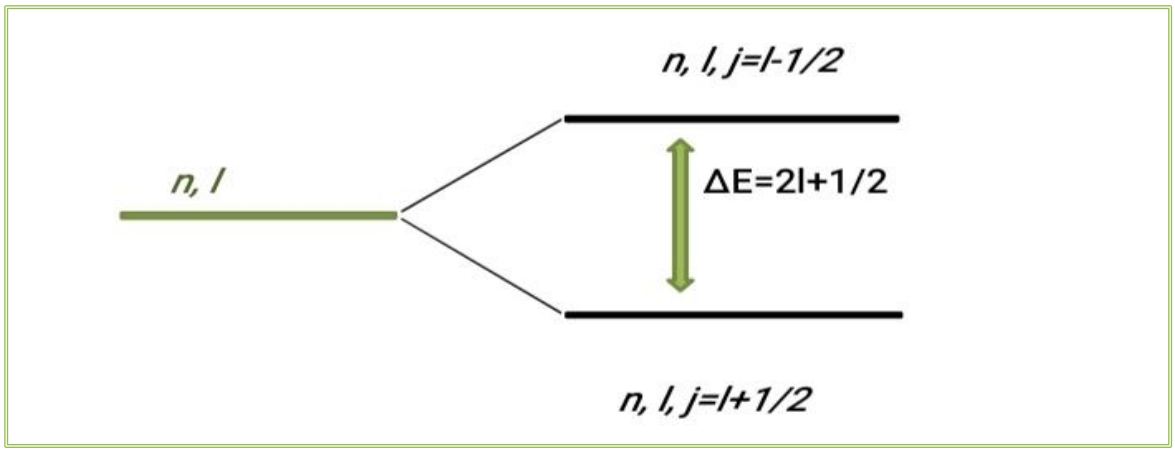

Figure I.1: Split up of states with ***n, l*** into states with ***n, l, j***.

The Hamiltonian using the spin-orbit interaction reproduced all the magic numbers. The obtained single-particle orbitals are represented on Figure I.2 [2].

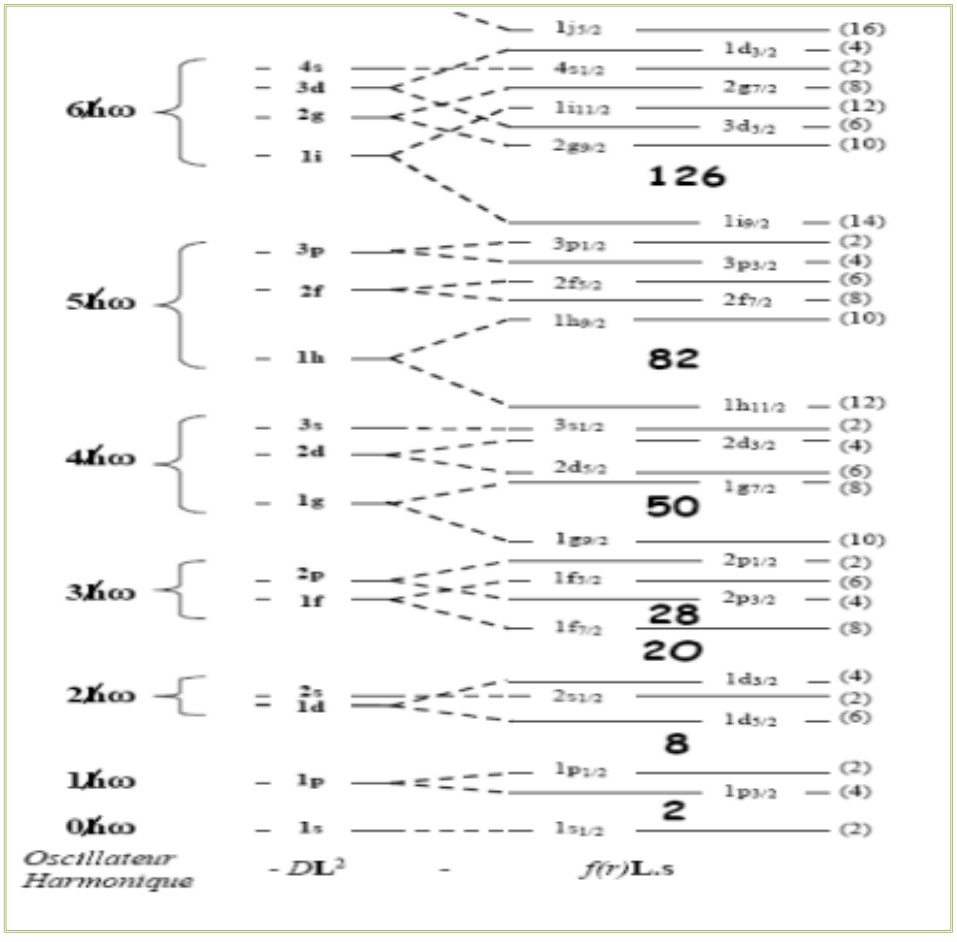

Figure I.2: Shell model single-particle orbitals [2].

I.3. Behind the mean field

The independent particles model is applicable only for spherical nuclei with single nucleon outside an inert core. The case of a nucleus with **A** interacting nucleons (**Z** protons and **N** neutrons), assumes that these nucleons interact in pairs with the two-body interaction **"Vij"**. The Hamiltonian of this nucleus has the form [2]:

$$H = \sum_{i=1}^{A}(T_i+U_i)+\left(\sum_{i>j}^{A} V_{ij} - \sum_{i=1}^{A} U_i\right) = H_0 + H_r = \sum_{i=1}^{A} h_i + H_r \quad \textbf{(11)}$$

H_0: The independent movement of nucleons in one body-potential.

h_i: The individual Hamiltonian of a nucleon.

H_r: The residual two-body interaction, which is considered as a perturbation of the main **H_0** Hamiltonian by an adequate choice.

II. Shell model ingredients

Any calculation of shell model requires the implementation of the following three ingredients [1]:

- Definition of a valence space (inert core, active shells).
- Derivation of a compatible effective interaction with the selected valence space.
- Calculation code to build and diagonalizable the Hamiltonians.

II.1. Choice of the valence space

In the shell model, the equation of Schrödinger relates to the so-called Hilbert space shown on Figure I.2, which led to a high matrix dimension. Thus, the Hilbert space is divided into three parts [1] shown on Figure I.3, which are:

1) **Inert core**: Composed of always-occupied shells, usually a magic nucleus having **Z_c** protons and **N_c** neutrons.
2) **Valence space:** which contains the rest of the active nucleons **(z=Z-Z_c)** and **(n=N-N_c)** which interact via the **H_r** interaction.
3) **External space:** formed of always unoccupied orbitals.

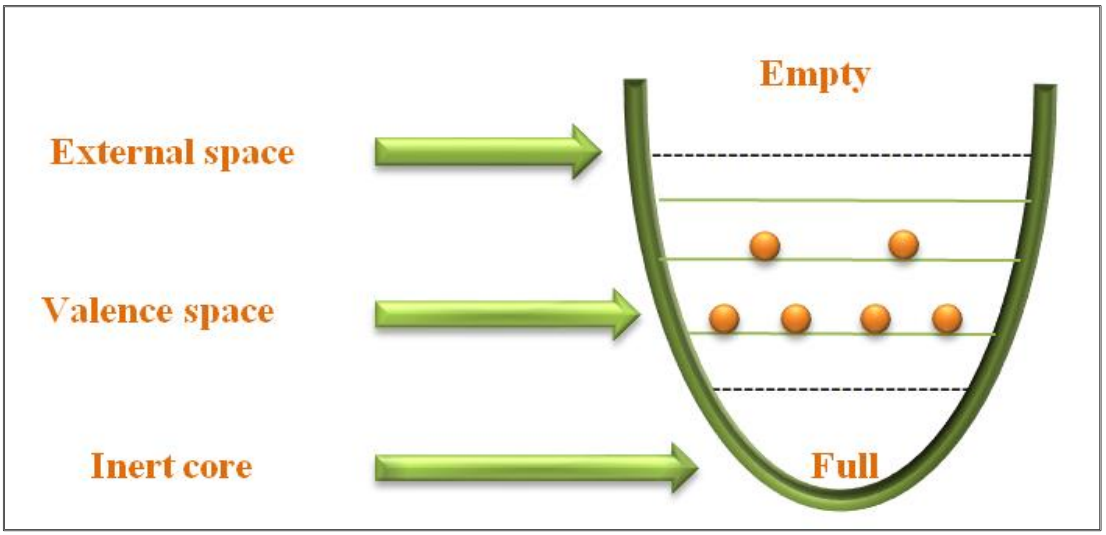

Figure I.3: Separation of the Hilbert space (see text for details).

As an example, we show on Figure I.4 the distribution of nucleons in ^{16}**O**, according to the single-particle orbitals (Figure I.2), and through the divided Hilbert space.

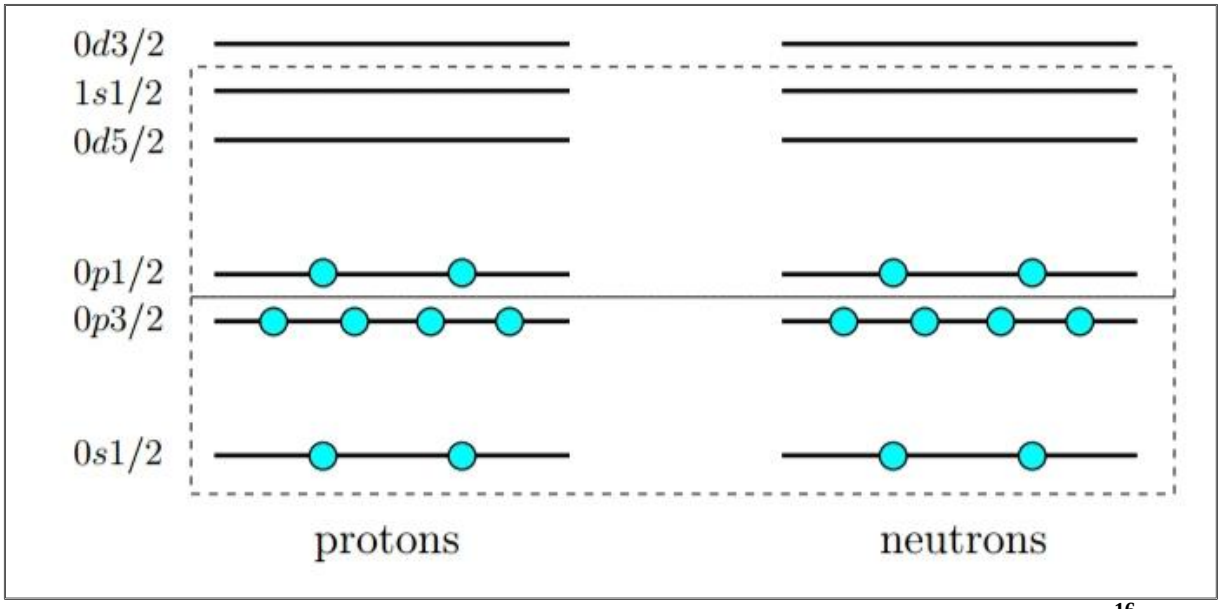

Figure I.4: Definition of the core and valence space necessary for the description of ^{16}**O**.

II.2. Effective interaction

Practically, any shell model calculation uses a "residual" or "effective" two-body interaction between valence nucleons. Because of the strong short-range repulsion, the free

nucleon-nucleon interaction cannot be used directly [1]. We have two types of effective interactions:

►The realistic effective interaction derived from nucleon-nucleon scattering potential.

►The phenomenological effective interaction extracted from fitting the matrix elements of a formed initial interaction to available experimental data.

II.3. Shell model codes

Several codes have been developed in order to carry out shell model calculations. To our knowledge, the most used codes are: GLASGOW [5], ANTOINE [6], VECSSE [7], MSHELL [8], REDSTICK [9], RITSSCHIL [10], OXBASH [11], DUPSM [12], and NATHAN [6, 13]. We will use in our calculations the code NATHAN.

III. Electromagnetic transitions in nuclear shell model

A nucleus formed in a nuclear reaction is generally in different excited states. If these states are bonded, their de-excitation towards the ground level is most often done by emission of gamma "**γ**" radiation [2]. The properties of the electromagnetic transitions may, in principle, be described by nuclear models and therefore provide interesting information on the validity of the calculated wave function of the states between which the transition is made [1].

During the transition of a nucleon between the initial level (of excitation energy $\mathbf{E_i}$, of angular momentum $\mathbf{J_i}$ and of parity $\boldsymbol{\pi_i}$) and the final level (of excitation energy $\mathbf{E_f}$, of angular momentum $\mathbf{J_f}$ and of parity $\boldsymbol{\pi_f}$), the nucleon emits a photon **γ** of energy $\mathbf{E_\gamma}$, of angular momentum **L** and of parity $\boldsymbol{\pi_\gamma}$ [2] (see Figure I.5), with:

$$E_\gamma = E_i - E_f, \quad |J_f - J_i| \leq L \leq J_f + J_i \text{ , and } \quad \pi_i \pi_\gamma \pi_f = 1 \qquad \textbf{(12)}$$

We note that the gamma transition between $\boldsymbol{J_i = J_f = 0}$ is forbidden by selection rules, because **L** for a photon is different of **0.**

The angular momentum of the transition is called also the multipolarity of the radiation. The character of the $\mathbf{2^L}$-pole is **dipolar** for **L=1, quadrupolar** for **L=2**, **octupolar** for **L=3**, **the multipole is of electric type EL** when $\boldsymbol{\pi_\gamma = (-1)^L}$ and **magnetic type ML** when

$\boldsymbol{\pi_\gamma}=(-\mathbf{1})^{L+1}$. Therefore, **"γ"** transitions that connect states of the same parities will get even **EL** and odd **ML**, those that connect states of different parities will have odd **EL** and even **ML** [2].

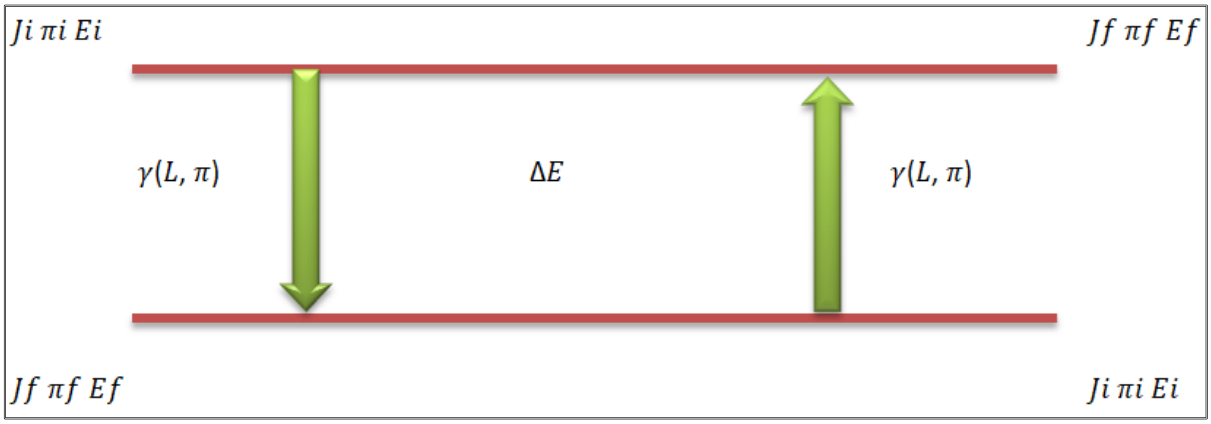

Figure I.5: Gamma emission and absorption in a nucleus.

III.1. *Operators*

III.1.1. Electric operator

The electric operator is given by the following formula [2]:

$$O_{LM}=\sum_{i=1}^{A} e(k)\, r^{L}(k)\, Y_{LM}(r\,(k)) \qquad \textbf{(13)}$$

Where e(k) denotes the free electric charge of a nucleon k, that equal:

$$\begin{cases} e(k)=0 \Rightarrow for\ neutrons \\ e(k)=e \Rightarrow for\ protons \end{cases}$$

III.1.2. Magnetic operator

The magnetic operator is given by the following formula [2]:

$$O_{LM}=\sum_{i=1}^{A} \mu_N \left[g^{s}(\mathrm{k})\ \vec{s}(\mathrm{k})+\frac{2g^{l}(k)}{L+1}\vec{l}(\mathrm{k})\right].\ \nabla\,(\mathrm{k})\, r^{l}(\mathrm{k})\, Y_{LM}(\mathrm{r}\,(\mathrm{k})) \qquad \textbf{(14)}$$

μ_N is the nuclear magneton given by $\mu_N=\frac{e\hbar}{2mc}$.

$\boldsymbol{g^{l}}$ **(k)** and $\boldsymbol{g^{s}}$**(k)** denote the orbital and spin gyromagnetic factors, respectively. In Table I.1 are presented the free orbital and spin **g** factors values [2].

TableI.1: free orbital and spin g factors values [2].

g(k)	Protons	neutrons
g^s**(k)**	5.586	-3.826
g^l**(k)**	1	0

III.2. *Probabilities of the electromagnetic transitions*

The reduced transition probabilities expressions are given by [2]:

$$B(EL) = \frac{9}{4\pi(L+3)^2} e^2 R^{2L} \frac{\Gamma_\gamma}{\Gamma_w} \qquad (e^2 fm^{2L}) \qquad \textbf{(15)}$$

$$B(ML) = \frac{90}{\pi(L+3)^2} \mu_N R^{2L-2} \frac{\Gamma_\gamma}{\Gamma_w} \qquad (\mu_N^2 fm^{2L-2}) \qquad \textbf{(16)}$$

Where: **R=1.2** $A^{1/3}$ **(fm),**

e: the electric charge

Γ_γ: Transition width

Γ_w: Weisskopf estimate (in **eV**)

We present the single-particle width (Weisskopf estimate) Γ_w **(w. µ.)** in Table I.2 [2]:

TableI.2: Single-particle width (Weisskopf estimate) Γ_w **(W. u.)** in **MeV** [2].

Electric	**Magnetic**
Γ_w**(E1)=68** $A^{2/3}$ E_γ^3	Γ_w**(M1)=21** E_γ^3
Γ_w**(E2)=4.9×10**$^{-5}$ $A^{4/3}$ E_γ^5	Γ_w**(M2)=1.5×10**$^{-5}$ $A^{2/3}$ E_γ^5
Γ_w**(E3)=2.3×10**$^{-11}$ A^2 E_γ^7	Γ_w**(M3)=6.8×10**$^{-12}$ $A^{4/3}$ E_γ^7
Γ_w**(E4)=6.8×10**$^{-18}$ $A^{8/3}$ E_γ^9	Γ_w**(M4)=2.1×10**$^{-18}$ A^2 E_γ^9
Γ_w**(E5)=1.6×10**$^{-24}$ $A^{10/3}$ E_γ^{11}	Γ_w**(M5)=4.9×10**$^{-25}$ $A^{8/3}$ E_γ^{11}

Notes:

1. The reduced probability of a transition **B (E2)** allows figuring out if the transition is due to an individual or collective contribution of nucleons in the nucleus. Indeed, the **B (E2)** is rather weak for a spherical nucleus and higher for a collective or deformed nucleus.
2. If the initial state decreases to different final states, then the total transition width $\boldsymbol{\Gamma_T}$ is the sum of the partial widths:

$$\Gamma_T = \sum_k \Gamma_{\gamma k} \qquad \textbf{(17)}$$

3. The half-life is given according to the mean life-time by:

$$T_{1/2} = \tau_m . \, ln2 \qquad \textbf{(18)}$$

IV. Isospin

Protons and neutrons have almost the same mass **(Mn/Mp=1.0014)**, the same spin **(s=1/2)**, and the same nuclear properties [2]. Hence, Heisenberg proposed that proton and neutron could be considered as two different charge states of the same particle, the nucleon. He introduced for each nucleon a new observable, which have the same properties as the spin, called isospin "***t"***, with $\boldsymbol{t = \frac{1}{2}}$. In order to distinguish between the two-nucleon types, he assumed two values of isospin projection on **oz** axis [2]:

$$\begin{cases} t_z = \dfrac{1}{2} \Rightarrow for\ neutron \\ t_z = -\dfrac{1}{2} \Rightarrow for\ proton \end{cases}$$

The isospin **T** and its projection, on **oz** axis, $\mathbf{T_Z}$ of a nucleus with (**A=Z+N**) nucleons is given by the following formulas:

$$T = \sum_1^A \vec{t_i} \ , \quad T_Z = \frac{(N-Z)}{2} \qquad \textbf{(19)}$$

The electric charge of a nucleus **Q**, thus, is related to $\mathbf{T_Z}$ by the following equation:

$$Q = \sum_1^Z q_i = Ze \ \Rightarrow \ Z = \frac{Q}{e} \ ; \quad T_Z = \frac{A}{2} - Z = \frac{A}{2} - \frac{Q}{e} \ \Rightarrow \ Q = (\frac{A}{2} - T_Z)\, e \qquad \textbf{(20)}$$

In this chapter, we have presented the basic concepts of nuclear shell model and electromagnetic transitions.

We will expose in the next chapter the proprieties of the **sd** shell nuclei and the **PSDPF** interaction.

Chapter II

Chapter II

sd shell nuclei and the PSDPF interaction

In recent years, the region of **sd** nuclei has been the interesting subject of many experimental and theoretical researches. This region of nuclei has particular behaviors and is characterized by the coexistence of certain properties.

In this subsection, we will expose some properties of the **sd** shell nuclei and we introduce the **PSDPF** interaction developed to reproduce the spectroscopic properties and the structure of these nuclei.

I. sd shell nuclei

The **sd** shell nuclei region is located between the two doubly-magic nuclei ^{16}**O** and ^{40}**Ca**, and thus have a number of protons **Z** and neutrons **N** comprise between 8 and 20 [1]. This area of nuclei, presented in Figure II.1, contains **146** experimentally known nuclei, **20** among them are stable.

In our thesis, we are interested in studying the structure of "^{26}**Al** and ^{27}**Al**", situated in the middle of the **sd** shell.

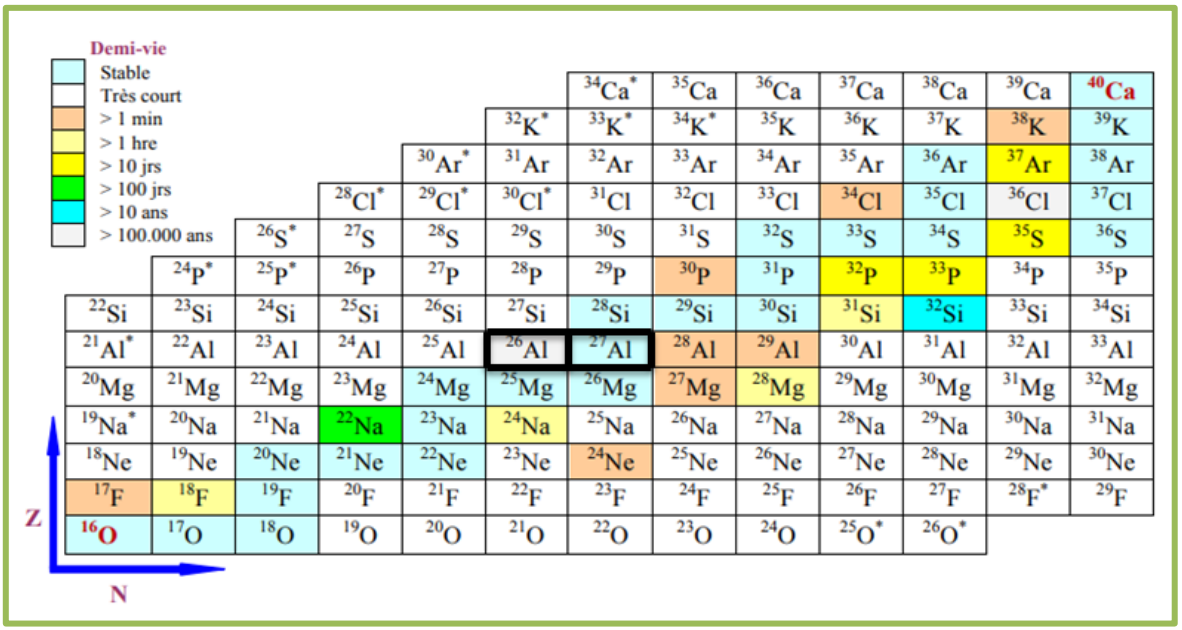

Figure II.1: Chart of the **sd** shell nuclei [14].

II. States in sd nuclei

II.1. Normal states

The **sd** shell nuclei possess spherical normal positive parity states that result from the distribution of the active nucleons within the **sd** shell with an ^{16}**O** inert core; hence the name of **0ħω** or 0 particle-0 hole (**0p-0h**) states. Their description is ensured using the well-known effective interactions (**USD** [15, 16] or **USDA/B** [17]).

II.2. Intruder states

In **sd** shell nuclei, two kinds of intruder states can exist with positive- or negative- parity. These states are different in their parities but have a common point that they result from the promotion of nucleons between major shells. We will examine separately the intruder positive- and negative- parity states.

- ✓ **Négative parity states**

These negative parity states, also called **1ħω** states, result from one nucleon jump (**1p-1h**) between two major shells **p-sd** or **sd-pf**. It is expected that the promotion of one nucleon from **p** to **sd** is for nuclei at the beginning of the **sd** shell and from **sd** to **pf** is for nuclei at the end of **sd** shell. At the middle of the **sd** shell, these states have a competition between the two excitations. Their description is not possible in the **sd** model space (**0ħω** space) but requires a larger space which contains the **p**, **sd** and **pf** major shells [1, 18]. The **sd** nuclei that possess experimentally observed **1ħω** intruder states are shown in Figure II.2.

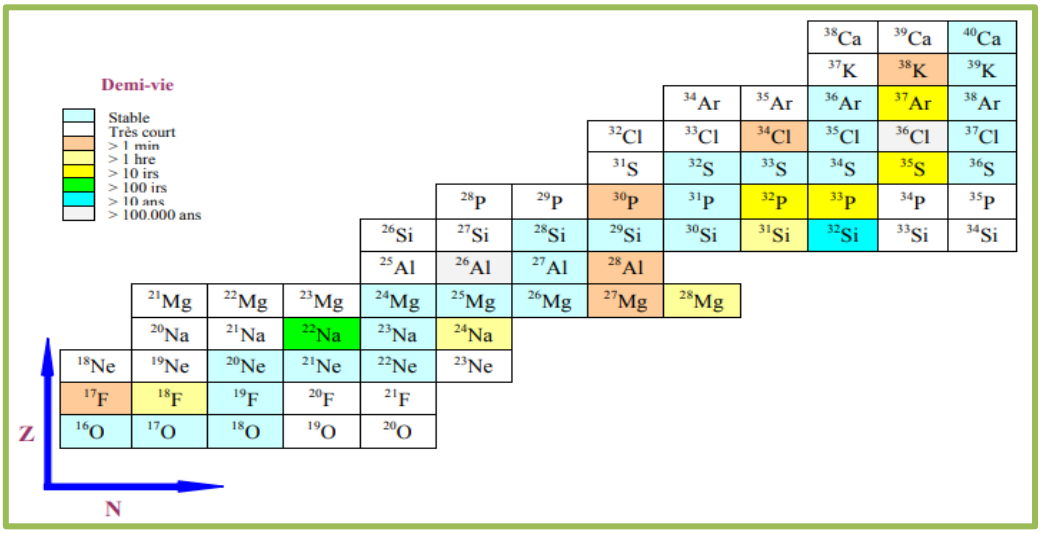

Figure II.2: Chart of sd nuclei with known negative parity intruder states [2].

✓ **Positive parity states**

sd nuclei can possibly have intruder states with positive parity whose configurations are outside the **sd** valence space. This type of levels has configurations of type **2p-2h**, **4p-4h**, which are generally deformed or even supper deformed (**SD**) with **8p-8h** configurations. These letter effects (**SD**) are observed near the doubly magic nuclei ^{16}**O** and ^{40}**Ca** [1, 18]. These (**np-nh,** with **n>3**) cannot be described even in the **p-sd-pf** valence space and requires more extended one.

III. PSDPF interaction

The shell model using **USD** interaction [15, 16] or the updated ones **USDA/B** [17] succeeded in the description of normal positive parity **(+)** states of sd nuclei within sd model space with an ^{16}**O** inert core. Furthermore, the **PSDPF** interaction was developed, in Strasbourg by M. Bouhelal [1, 18], in order to describe simultaneously both types of the spherical **(0+1) ħω** states in the sd shell nuclei as well as the transitions issued from the different parity states. In this case, the model space is composed of **3** major shells **p**, **sd** and **pf** containing the following **9** sub-shells: $\mathbf{1}p_{3/2}$, $\mathbf{1}p_{1/2}$, $\mathbf{1}d_{5/2}$, $\mathbf{2}s_{1/2}$, $\mathbf{1}d_{3/2}$, $\mathbf{1}f_{7/2}$, $\mathbf{2}p_{3/2}$, $\mathbf{1}f_{5/2}$ and $\mathbf{2}p_{1/2}$, with a ^{4}**He** inert core.

The **PSDPF** interaction describes consistently the normal and intruder parity states throughout the entire **sd** shell.

✓ **Application of PSDPF interaction**

In recent years, there has been much experimental and theoretical work on the structure of nuclei at low excitation energies close to the valley of stability, such as the **sd** shell nuclei area. Among of the theoretical work, the shell model framework employing the **PSDPF** interaction has a great success in describing the **(0+1) ħω** states in nuclei throughout the **sd** shell.

PSDPF interaction has been used to calculate the spectroscopic properties (energy spectra and electromagnetic transitions) of several **sd** nuclei and chains: **sulfur** [19-25], **phosphorus** [20, 26-28], **silicon** [20, 29-33] and other **sd** nuclei such as ^{22,23}**Na** [34, 35], ^{22}**Mg** [36] and **0**$^{-,+}$ [37,38].

In addition, **PSDPF** has been used to explain many experimental results on energy spectra and electromagnetic transitions of many **sd** nuclei and chains: **sulfurs** [39-43], **phosphorus** [42, 44-46], **silicon** [47], **chlorine** [48-50], Argon [51], ^{23,24}**Mg** and ^{23}**Na** [52, 53].

All of these previous studies have given more credit to the PSDPF interaction.

IV. Shell model ingredients for sd shell nuclei

- Valence space: the full **p-sd-pf** space.
- Compatible interaction with this space: **PSDPF** interaction.
- Code of calculation: the shell model code **NATHAN** [6, 13].

✓ **Nucleons distributions in ^{27}Al**

As an example, we used the **PSDPF** interaction to calculate the probabilities of distributing neutrons and protons (their shell occupations) in ^{27}**Al** that gives rise the first + and – states as **1/2**$^{+}$ and **1/2**$^{-}$, respectively. The obtained results are shown on Tables II.1 and II.2 for the **1/2**$^{+}$ and **1/2**$^{-}$ states, respectively. Note that the configurations of both states are fragmented due to the almost high valence nucleons number, **5** protons, and **6** neutrons outside ^{16}**O**. In this ^{27}**Al** nucleus, the ground state is **5/2**$^{+}$ corresponding to the fulfilling of the neutron $\mathbf{1d_{5/2}}$ sub-shell, and to a proton hole in $\mathbf{1d_{5/2}}$. As it can be seen, the **1/2**$^{+}$ state has the most probable configuration, $\mathbf{(1d_{5/2})^4(2s_{1/2})^1}$ for protons and fulfilling neutron $\mathbf{1d_{5/2}}$. Concerning the intruder **1/2**$^{-}$ state, its most probable configuration corresponds to the promotion of a proton from $\mathbf{1p_{1/2}}$ to $\mathbf{1d_{5/2}}$ sub-shells. Figure II.4 presents the shell occupations of the first excited positive- and negative parity states, **1/2**$^{+}$ and **1/2**$^{-}$, in ^{27}**Al**.

Table II.1: Shell occupation probabilities of $1/2^+$ states of ^{27}Al.

		Neutron distribution									Proton distribution								
Probability		1p 1/2	1p 3/2	1d 5/2	2s ½	1d 3/2	1f 7/2	2p 3/2	1f 5/2	2p 1/2	1p 1/2	1p 3/2	1d 5/2	2s 1/2	1d 3/2	1f 7/2	2p 3/2	1f 5/2	2p ½
$1/2^+$ states	0.01031117	2	4	2	1	2	0	0	0	0	2	4	3	2	1	0	0	0	0
	0.01231371	2	4	2	1	2	0	0	0	0	2	4	4	1	1	0	0	0	0
	0.01367828	2	4	2	1	2	0	0	0	0	2	4	4	2	0	0	0	0	0
	0.01093252	2	4	2	1	2	0	0	0	0	2	4	5	1	0	0	0	0	0
	0.01112141	2	4	3	0	2	0	0	0	0	2	4	4	1	1	0	0	0	0
	0.01291331	2	4	3	0	2	0	0	0	0	2	4	5	1	0	0	0	0	0
	0.01145166	2	4	3	1	1	0	0	0	0	2	4	2	2	2	0	0	0	0
	0.02791139	2	4	3	1	1	0	0	0	0	2	4	3	2	1	0	0	0	0
	0.01003624	2	4	3	1	1	0	0	0	0	2	4	4	0	2	0	0	0	0
	0.02483490	2	4	3	1	1	0	0	0	0	2	4	4	1	1	0	0	0	0
	0.02424139	2	4	3	1	1	0	0	0	0	2	4	4	2	0	0	0	0	0
	0.01332255	2	4	3	1	1	0	0	0	0	2	4	5	0	1	0	0	0	0
	0.02233924	2	4	3	1	1	0	0	0	0	2	4	5	1	0	0	0	0	0
	0.01225532	2	4	4	0	1	0	0	0	0	2	4	3	1	2	0	0	0	0
	0.01021058	2	4	4	0	1	0	0	0	0	2	4	3	2	1	0	0	0	0
	0.03665703	2	4	4	0	1	0	0	0	0	2	4	4	1	1	0	0	0	0
	0.02225245	2	4	4	0	1	0	0	0	0	2	4	5	1	0	0	0	0	0
	0.01600166	2	4	4	1	0	0	0	0	0	2	4	2	2	2	0	0	0	0
	0.02125158	2	4	4	1	0	0	0	0	0	2	4	3	2	1	0	0	0	0
	0.01169202	2	4	4	1	0	0	0	0	0	2	4	4	1	1	0	0	0	0
	0.04793470	2	4	4	1	0	0	0	0	0	2	4	4	2	0	0	0	0	0
	0.01849414	2	4	4	1	0	0	0	0	0	2	4	5	0	1	0	0	0	0
	0.01087203	2	4	4	1	0	0	0	0	0	2	4	5	1	0	0	0	0	0
	0.12217495	2	4	4	1	0	0	0	0	0	2	4	6	0	0	0	0	0	0
	0.01236868	2	4	5	0	0	0	0	0	0	2	4	3	1	2	0	0	0	0
	0.01466066	2	4	5	0	0	0	0	0	0	2	4	3	2	1	0	0	0	0
	0.02431410	2	4	5	0	0	0	0	0	0	2	4	4	1	1	0	0	0	0
	0.01302987	2	4	5	0	0	0	0	0	0	2	4	4	2	0	0	0	0	0
	0.04214593	2	4	5	0	0	0	0	0	0	2	4	5	1	0	0	0	0	0

.

Table II.2: Shell occupation probabilities of $1/2^{-}$ states of ^{27}Al

		Neutron distribution									Proton distribution								
Probability		$1p_{1/2}$	$1p_{3/2}$	$1d_{5/2}$	$2s_{1/2}$	$1d_{3/2}$	$1f_{7/2}$	$2p_{3/2}$	$1f_{5/2}$	$2p_{1/2}$	$1p_{1/2}$	$1p_{3/2}$	$1d_{5/2}$	$2s_{1/2}$	$1d_{3/2}$	$1f_{7/2}$	$2p_{3/2}$	$1f_{5/2}$	$2p_{1/2}$
$1/2^{-}$ states	0.01383761	1	4	3	2	1	0	0	0	0	2	4	3	2	1	0	0	0	0
	0.01172737	1	4	4	1	1	0	0	0	0	2	4	3	2	1	0	0	0	0
	0.02148607	1	4	4	1	1	0	0	0	0	2	4	4	1	1	0	0	0	0
	0.01093265	1	4	4	1	1	0	0	0	0	2	4	4	2	0	0	0	0	0
	0.01312064	1	4	4	1	1	0	0	0	0	2	4	5	1	0	0	0	0	0
	0.01082064	1	4	4	2	0	0	0	0	0	2	4	3	2	1	0	0	0	0
	0.01026979	1	4	4	2	0	0	0	0	0	2	4	4	1	1	0	0	0	0
	0.02403441	1	4	4	2	0	0	0	0	0	2	4	4	2	0	0	0	0	0
	0.01686547	1	4	4	2	0	0	0	0	0	2	4	6	0	0	0	0	0	0
	0.01539182	1	4	5	0	1	0	0	0	0	2	4	5	0	1	0	0	0	0
	0.01491820	1	4	5	1	0	0	0	0	0	2	4	3	2	1	0	0	0	0
	0.01649684	1	4	5	1	0	0	0	0	0	2	4	4	1	1	0	0	0	0
	0.03949571	1	4	5	1	0	0	0	0	0	2	4	5	1	0	0	0	0	0
	0.01461055	1	4	6	0	0	0	0	0	0	2	4	4	0	2	0	0	0	0
	0.01243660	1	4	6	0	0	0	0	0	0	2	4	4	1	1	0	0	0	0
	0.02743113	1	4	6	0	0	0	0	0	0	2	4	4	2	0	0	0	0	0
	0.06381045	1	4	6	0	0	0	0	0	0	2	4	6	0	0	0	0	0	0
	0.01324945	2	3	5	0	1	0	0	0	0	2	4	6	0	0	0	0	0	0

.

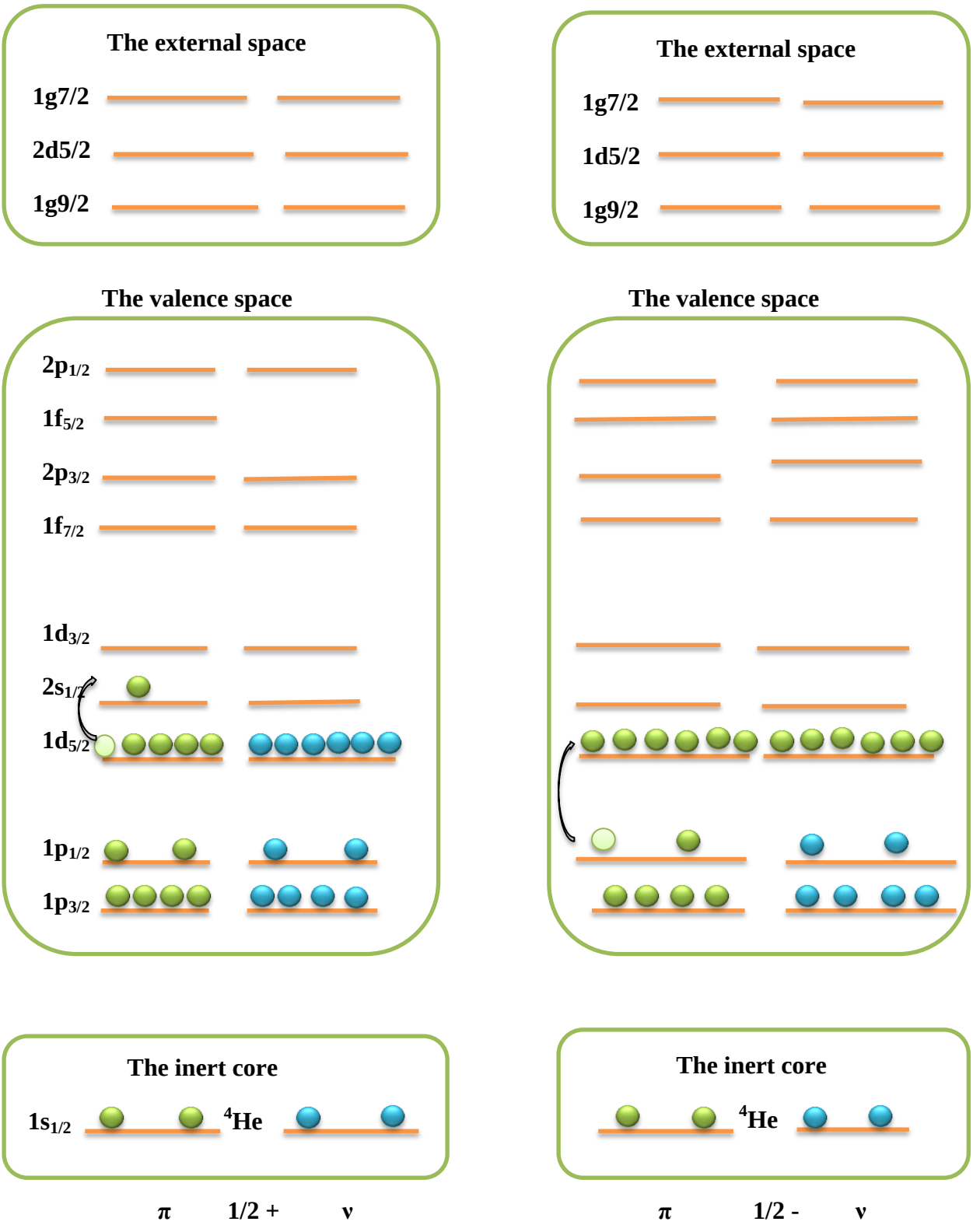

FigureII.3: Schematic distribution of the first excited levels $1/2^{+}$ and $1/2^{-}$ in ^{27}Al.

III. Electromagnetic transitions in sd nuclei

The **PSDPF** interaction succeeded in the description of the **(0+1) ħω** states in **sd** shell nuclei. Electromagnetic transitions are a useful test of the wave functions of each developed interaction. As it was mentioned previously, the electromagnetic transitions operators need the effective charges and gyromagnetic factors parameters. Transitions between positive parity states **E2** and **M1** have been studied using **USDA/B** interactions [54]. Transitions connecting opposite parity states, **E1**, **M2** and **E3**, can be studied using the **(0+1) ħω PSDPF** interaction.

M. LABIDI has studied the **E3** transitions by adjusting its effective charges to available experimental values [24, 55]. The obtained parameters for the three **E2**, **M1** and **E3** transitions are presented on Table II.3.

Table II.3: Adjusted parameters for the transitions **E2**, **M1** and **E3**.

W. A. Richter and B. A. Brown [54]		**M. Labidi [24, 55]**
Effective charges (E2)	**Gyromagnetic factors (M1)**	**Effective charges (E3)**
e_p = 1.36	g^l_p = 1.159	e_p = 1.36
	g^s_p = 5.150	
e_n = 0.45	g^l_n = −0.090	e_n = 0.48
	g^s_n = −3.550	

In this chapter, we defined the **sd** shell nuclei and we present an overview of the interactions developed to reproduce their spectroscopic properties and structure. The last part of this chapter was dedicated to the electromagnetic transitions in **sd** shell nuclei.

As an application of the **PSDPF** interaction, we will present in the last chapter a detailed discussion of the comparison of our results concerning ^{26,27}**Al** structures to the available experimental data.

Chapter III

Chapter III

Spectroscopic properties of ^{26}Al and ^{27}Al

In the two previous chapters, we presented a brief review about the nuclear shell model and the properties of sd shell nuclei and **PSDPF i**nteraction. In this chapter, we will use the **PSDPF** interaction and the code Nathan to calculate the energy spectra of **^{26}Al** and **^{27}Al** then compared them to the experimental ones. Our purpose is the precise examination of the experimental spectrum of each of the isotopes in question in order to determine the ambiguous states based also from the calculated electromagnetic transitions. The results of our study will be presented and discussed after a short experimental review of each isotope.

I. Experimental review of ^{26}Al and ^{27}Al energy spectra

I.1. Case of ^{26}Al

Frisch et al., reported that the first observation of **^{26}Al** was in 1934 [56]. The **^{26}Al** is a **self-conjugate** (**N = Z**) **sd** shell nucleus and therefore it has **T = 0** and **T = 1** states that makes its spectrum very condensed with high density states. Their latest adopted levels were published in 2016 [14, 57]. Its spectrum contains, up to **~ 7.6 MeV**, **139** states including **92** unconfirmed states, among them **71** states with uncertain **J^{π}** and **21** with known parity and uncertain **J**. There are many degenerate states in the spectrum of **^{26}Al** [14, 57]. For example, there are **3** degenerate levels observed at **~ 2.07 MeV**; with **$J^{\pi} = 4^{+}$** at **2.069 MeV**, **$J^{\pi} = 2^{+}$** at **2.070 MeV**, and **$J^{\pi} = 1^{+}$** at **2.072 MeV**.

I.2. Case of ^{27}Al

Aston identified the **^{27}Al**, with **N > Z**, in 1922 as reported in Ref. [56]. The updated adopted levels of **^{27}Al** were published in 2011 [14, 58]. Its spectrum comprises, up to **~ 10 keV**, **157** states; among them **120** unconfirmed states and **28** states with unknown **J^{π}**.

II. Results and discussion

We performed a shell model calculation using the **PSDPF** interaction to describe the energy spectra of the ^{26}**Al** and ^{27}**Al**. The comparison to available experimental data allowed us to confirm and determine the $\mathbf{J^{\pi}}$ assignments of the uncertain and unknown states, respectively. This calculation has been done using the shell model code Nathan. In order to confirm the $\mathbf{J^{\pi}}$ assignments of the first excited states in ^{27}**Al**, we calculated also their half-lives and compared them to experiment.

II.1. Energy spectrum

We present a detailed discussion of our results separately in the both cases of ^{26}**Al** and ^{27}**Al**.

- **Case of ^{26}Al**

The ^{26}**Al** is a self-conjugate nucleus with **N = Z** and therefor it has two types of states, **T = 0** and **T = 1**. States with **T = 1** can be obtained by comparing the excitation energies in the **A=26** isobaric triplet ^{26}**Mg**, ^{26}**Si** and ^{26}**Al**. The comparison of the calculated versus experimental [14] excitation energies, up to **~ 7.6 MeV**, as well as the experimental [14] **T = 1** states in ^{26}**Mg** and ^{26}**Si** are presented in Table III. 1. The ground state of ^{26}**Al** has a **T = 0** and a $\mathbf{J^{\pi} = 5^{+}}$ while its first excited state, observed at 228.3 keV, has a **T = 1** and a $\mathbf{J^{\pi} = 0^{+}}$. This ($\mathbf{J^{\pi} = 0^{+}}$, **T = 1**) state is the ground state in the mirror nuclei ^{26}**Mg** and ^{26}**Si**. All the **T = 1** states are reported in the last column. In this Table, **ΔE** denotes the energy difference between theory and experiment, i.e. **ΔE = Eth - Eexp**.

We can see that the **PSDPF** interaction describes quite well the **0** and **1ħω** states of the studied nucleus. Some discrepancies between calculation and experiment have been found and are interpreted as follows:

1. The first excited positive parity state observed at 228 KeV is not well reproduced.
2. States with **ΔE > 400 keV** (in red color), have a collective contribution with more than 0p-0h or 1p-1h configurations for + or – states, respectively), and those with **ΔE ~ 1 MeV** are pure collective states.
3. States with **ΔE < – 400 keV** (in blue color), are not well reproduced using **PSDPF**.

Table III. 1: Comparison experimental [14] versus theory of the energy spectra of ^{26}**Al.**

J^{π}_{exp}	^{26}Al	J^{π}_{i}	Eth	ΔE	^{26}Al	^{26}Mg	^{26}Si	T=1 States
5^+	0	5^+_1	0	0	-0.228			
0^+	0.228	0^+_1	0.072	-0.156	0	0	0	T=1
3^+	0.417	3^+_1	0.557	0.140	0.189			
1^+	1.058	1^+_1	1.071	0.013	0.830			
2^+	1.759	2^+_1	1.817	0.058	1.531			
1^+	1.851	1^+_2	1.832	-0.019	1.623			
(4^+)	2.069	4^+_1	2.118	0.049	1.841			
(2^+)	2.070	2^+_2	1.950	-0.120	1.842	1.809	1.797	T=1
1^+	2.072	1^+_3	2.248	0.176	1.844			
3^+	2.365	3^+_2	2.124	-0.241	2.137			
3^+	2.545	3^+_3	2.524	-0.021	2.317			
2^+	2.661	2^+_3	2.684	0.023	2.433			
1^+	2.740	1^+_4	2.828	0.088	2.512			
2^+	2.913	2^+_4	2.967	0.054	2.685			
3^+	3.074	3^+_4	3.176	0.102	2.846			
2^+	3.160	2^+_5	3.114	-0.046	2.932	2.938	2.787	T=1
5^+	3.403	5^+_2	3.428	0.025	3.175			
6^+	3.508	6^+_1	3.441	-0.067	3.280			
3^+	3.596	3^+_5	3.353	-0.243	3.368			
4^+	3.675	4^+_2	3.670	-0.005	3.447			
3^+	3.681	3^+_6	3.491	-0.190	3.453			
1^+	3.724	1^+_5	3.518	-0.206	3.496			
2^+	3.751	2^+_6	3.877	0.126	3.523			
0^+	3.754	0^+_2	3.900	0.146	3.526	3.589	3.336	T=1
7^+	3.922	7^+_1	3.812	-0.110	3.694			
(3^+)	3.963	3^+_7	4.029	0.066	3.735			
0^-	3.978	0^-_1	3.254	-0.724	3.750			
(3^+)	4.192	3^+_8	4.062	-0.130	3.964	3.942	3.758	T=1
(4^+)	4.206	4^+_3	3.975	-0.231	3.978			
3^+	4.349	3^+_9	4.426	0.077	4.121			
2^-	4.431	2^-_1	2.779	-1.652	4.203			
0^-	4.481	0^-_2	5.551	1.070	4.253			
2^+	4.548	2^+_7	4.662	0.114	4.320	4.333	4.139	T=1
(3^+)	4.599	3^+_{10}	4.461	-0.138	4.371	4.350	4.188	T=1
(2^-)	4.622	2^-_2	4.307	-0.315	4.394			
(4^+)	4.705	4^+_4	4.469	-0.236	4.477	4.319	4.446	T=1
4^+	4.773	4^+_5	4.861	0.088	4.545			
(1^-)	4.940	1^-_1	3.775	-1.165	4.712			
(5^+)	4.941	5^+_3	4.809	-0.132	4.713			
(3^+)	4.952	3^+_{11}	4.996	0.044	4.724			
(2^-)	5.007	2^-_3	5.142	0.135	4.779			
(1^+)	5.010	1^+_6	4.938	-0.072	4.782			
(4^+)	5.132	4^+_6	5.085	-0.047	4.904	4.901	4.797	T=1
$2^{+(a)}$	5.142	2^+_8	5.016	-0.126	4.914	4.835	4.811	T=1
(0^+)	5.195	0^+_3	4.981	-0.214	4.967	4.972	4.831	T=1
(4^+)	5.245	4^+_7	5.262	0.017	5.017			
(4^-)	5.396	4^-_1	4.990	-0.406	5.168			
(1^-)	5.431	1^-_2	4.898	-0.533	5.203			
(3^-)	5.457	3^-_1	4.425	-1.032	5.229			
0^+, (1, 2)	5.462	0^+_4	5.179	-0.283	5.234			
0^+, (1, 2)	5.462	1^+_7	5.171	-0.291	5.234			

5^+, (4^-)	5.488	5^+_4	5.331	-0.157	5.260			
5^+, (4^-)	5.488	4^-_2	5.319	-0.169	5.260			
(2^+)	5.495	2^+_9	5.351	-0.144	5.267			
(4^+)	5.513	4^+_8	5.625	0.112	5.285			
(2^+)	5.545	2^+_{10}	5.572	0.027	5.317	5.292	5.148	T=1
(4, 5)	5.569	5^+_5	5.624	0.055	5.341			
(1)	5.585	1^+_8	5.765	0.180	5.357			
$(2, 3)^-$	5.598	3^-_2	5.354	-0.244	5.370			
$(2, 3)^-$	5.598	2^-_4	5.353	-0.245	5.370			
1^+	5.671	1^+_9	5.913	0.242	5.443			
(4^-)	5.676	4^-_3	5.742	0.066	5.448			
(3^-)	5.692	3^-_3	5.840	0.148	5.464			
(4^+)	5.726	4^+_9	5.645	-0.081	5.498	5.476	5.289	T=1
(2^+)	5.849	2^+_{11}	5.769	-0.080	5.621			
(3^+)	5.883	3^+_{12}	6.355	0.472	5.655			
(2^-)	5.916	2^-_5	5.793	-0.123	5.688			
(4^+)	5.924	4^+_{10}	5.997	0.073	5.696	5.716	5.518	T=1
$1^{(+)}$	5.950	1^+_{10}	6.245	0.295	5.722			
(1^+)	6.028	1^+_{11}	6.739	0.711	5.800	5.691	5.676	T=1
(5^-)	6.084	5^-_1	5.761	-0.323	5.856			
(5^-)	6.084	5^+_6	6.078	-0.006	5.856			
$(1^-, 2^+)$	6.086	1^-_3	5.808	-0.278	5.858			
$(4 \text{ TO } 6)^+$	6.120	6^+_2	6.157	0.037	5.892			
$(4 \text{ TO } 6)^+$	6.120	4^+_{11}	6.156	0.036	5.892			
$(1, 2^+)$	6.198	2^+_{12}	6.167	-0.031	5.970			
(1)	6.238	1^-_4	6.286	0.048	6.010			
(3^-)	6.254	3^-_4	5.880	-0.374	6.026			
1^+	6.270	1^+_{12}	6.821	0.551	6.042			
(3^+)	6.280	3^+_{13}	6.355	0.075	6.052			
(3^-)	6.343	3^-_5	6.139	-0.204	6.115			
(3^+)	6.364	3^+_{14}	6.418	0.054	6.136	6.125	5.929	T=1
$2^{-(a)}$	6.399	2^-_6	6.019	-0.380	6.171			
$(0 \text{ TO } 2^+)$	6.414	0^+_5	6.350	-0.064	6.186	6.256	5.946	T=1
$(0 \text{ TO } 2^+)$	6.414	2^+_{13}	6.338	-0.076	6.186	6.483	6.259	T=1
$(3 \text{ TO } 5^+)$	6.436	5^+_7	6.201	-0.235	6.208			
$(3 \text{ TO } 5^+)$	6.496	5^+_8	6.686	0.190	6.268			
$(4^+, 5^-)$	6.551	5^-_2	6.609	0.058	6.323			
(5^+)	6.598	5^+_9	6.855	0.257	6.370			
(3^-)	6.610	3^-_6	6.615	0.005	6.382			
(2^+)	6.680	2^+_{14}	6.740	0.060	6.452			
(7)	6.695	7^+_2	6.545	-0.150	6.467			
(4^-)	6.724	4^-_4	6.377	-0.347	6.496			
(2^-)	6.784	2^-_7	6.635	-0.149	6.556			
(3^-)	6.789	3^-_7	6.788	-0.001	6.561			
(3^+)	6.801	3^+_{15}	7.020	0.219	6.573			
1^+, $(1^-, 2^-)$	6.802	1^+_{13}	6.901	0.099	6.574			
1^+, $(1^-, 2^-)$	6.802	1^-_5	6.473	-0.329	6.574			
6^+, (4, 5)	6.816	6^+_3	6.779	-0.037	6.588			
(4^+)	6.818	4^+_{12}	6.887	0.069	6.590	6.623	6.765	T=1
(2^+)	6.852	2^+_{15}	7.008	0.156	6.624			
1^+	6.874	1^+_{14}	7.530	0.656	6.646			
(2^+)	6.876	2^+_{16}	7.027	0.151	6.648	6.745	6.383	T=1
(6^-)	6.892	6^-_1	6.241	-0.651	6.664			
(1^+)	6.936	1^-_6	6.601	-0.335	6.708			
(3^-)	6.964	3^-_8	7.058	0.094	6.736	6.876	6.787	T=1

(2^+)	7.001	2^+_{17}	7.286	0.285	6.773			
(5^+)	7.015	5^-_3	6.843	-0.172	6.787			
(3^+)	7.051	3^+_{16}	7.259	0.208	6.823			
1^-	7.086	1^-_7	6.734	-0.352	6.858	7.062	6.81	T=1
(2^+)	7.093	2^+_{18}	7.467	0.374	6.865			
$(4)^-$	7.109	4^-_5	6.545	-0.564	6.881			
$(2)^-$	7.142	2^-_8	6.821	-0.321	6.914			
$(3)^+$	7.153	3^+_{17}	7.317	0.164	6.925			
$(3)^-$	7.161	3^-_9	7.337	0.176	6.933			
$(4)^-$	7.168	4^-_6	7.090	-0.078	6.940			
1^+	7.198	1^+_{15}	7.626	0.428	6.970			
(5^+)	7.222	5^+_{10}	7.158	-0.064	6.994	6.978	7.198	T=1
$(3)^-$	7.238	3^-_{10}	7.583	0.345	7.010			
$(2)^-$	7.254	2^-_9	6.961	-0.293	7.026	6.952		T=1
0^-, (1, 2)	7.286	0^-_3	6.842	-0.444	7.058			
(4, 3)$^+$	7.291	4^+_{13}	6.953	-0.338	7.063			
(2^+)	7.308	2^+_{19}	7.646	0.338	7.080	7.100	7.154	T=1
$(4)^-$	7.348	4^-_7	7.386	0.038	7.120	7.261		T=1
(5^+)	7.366	5^+_{11}	7.185	-0.181	7.138			
$(2)^+$	7.397	8^+_1	7.397	0	7.169			
$(3)^-$	7.399	5^-_4	7.151	-0.248	7.171		7.522	T=1
$(4)^-$	7.410	4^-_8	7.664	0.254	7.182	7.283		T=1
$(4)^+$	7.425	4^+_{14}	7.378	-0.047	7.197			
0, (1, 2)	7.440	0^-_4	7.304	-0.136	7.212			
$(1)^-$	7.444	1^-_8	7.143	-0.301	7.216			
1^+	7.455	1^+_{16}	7.858	0.403	7.227			
(3^+)	7.464	3^+_{18}	7.730	0.266	7.236			
$(3)^+$	7.495	3^+_{19}	7.977	0.482	7.267	7.246	7.018	T=1
$(2)^-$	7.497	2^-_{10}	7.249	-0.248	7.269			
(6^-)	7.529	6^-_2	7.380	-0.149	7.301			
$(2)^-$	7.540	2^-_{11}	7.485	-0.055	7.312	7.542	7.606	T=1
(5^-)	7.548	5^-_5	7.651	0.103	7.320			
$(2)^+$	7.558	6^+_4	7.542	-0.016	7.330			

[a] **J^π** assignments taken from Ref. [59].

From this comparison, we can extract the following comments:

4. There is a one to one correspondence states between theory and experiment.
5. All the positive parity states were quite well reproduced whereas some of negative parity are predicted lower in energy than experiment.
6. All the uncertain **J^π** (in parenthesis) were confirmed. Some of them were defined with other **J^π** than the proposed ones; like the case of the last observed state at **7.558 MeV** with a proposed **$J^\pi = (2^+)$** but it is close to the **6^+_4** calculated state at **7.542 MeV**.
7. The undefined **J^π** states were assigned.
8. Several degenerate states with more that one **J^π** value, have been observed. As an example, we cite the case at **5.462 MeV**, with a proposed **$J^\pi = 0^+$, (1, 2)**, for which we attributed **$J^\pi = 0^+_4$** and **1^+_7**; according to their good energies calculated also at the same

values of **5.462 MeV**. All these excitation energy states are colored in red in 2nd column.

9. In addition, there is a state observed at **6.084 MeV**, with a proposed $\mathbf{J^{\pi}} = (\mathbf{5^-})$ which corresponds to the $\mathbf{5^-_1}$ calculated at **5.761 MeV**. However this observed state is close also to the $\mathbf{5^+_6}$ calculated at **6.078 MeV**, we think this state is also degenerate.
10. There are no $\mathbf{7^-}$ observed states between **0** and **7.6 MeV** in ^{26}**Al**; also the 7^-_1 is calculated at **7.765 MeV**.

In order to illustrate the good agreement experiment versus theory, we calculated the **R**oot **M**ean **S**quare **D**eviation "**rmsd**" for all states, and for the positive (**0ħω**) and negative (**1ħω**) states that are separately recorded in the Table III. 2 for ^{26}**Al** by applying the following formula:

$$rmsd = \sqrt{\frac{1}{n}\sum_{i=1}^{n}\left(E^{i}_{cal} - E^{i}_{\exp}\right)^{2}}$$

We remark that the calculated **rmsd** have low values for the two first treated cases, which proves that, the results obtained using **PSDPF** agree very well with the experimental ones. Nevertheless, some of the **1ħω** states are predicted lower in energy than experiment with an **rmsd = 462 keV**.

We present in Figure III. 1 the energy difference, **ΔE**, for the first positive and negative $\mathbf{J^{\pi}}$ states. All the **0ħω** states are in good agreement with experiment, which not the case for some of the **1ħω** states.

Table III. 2: The **rmsd** values (in keV) in ^{26}**Al**.

States	All states	0ħω states	1ħω states
rmsd	321	211	462

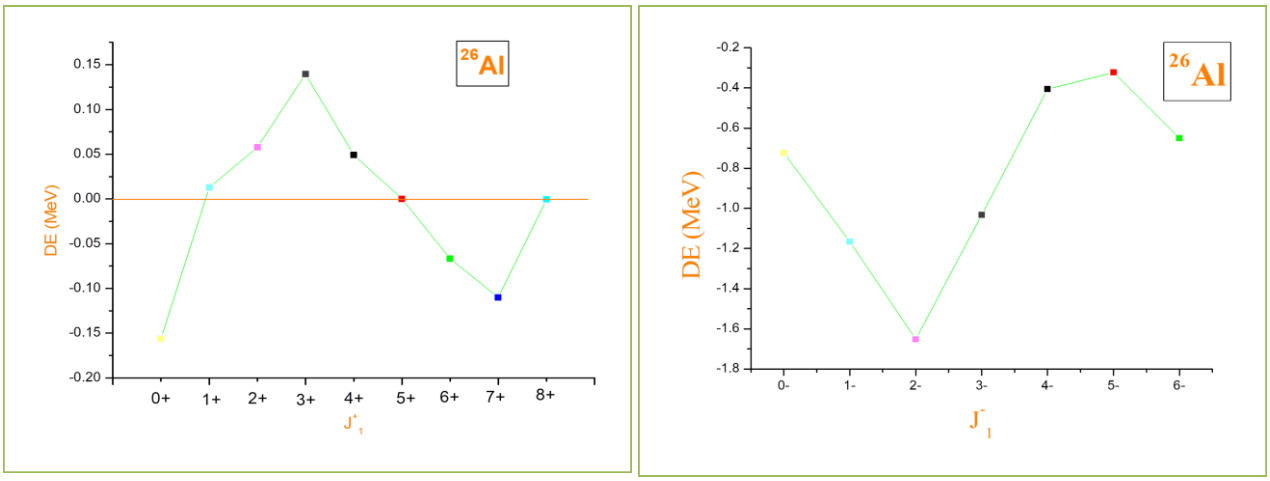

Figure III. 1: Energy difference, **ΔE**, for the first J^+ and J^- states in ^{26}**Al**.

➢ Case of ^{27}Al

The ^{27}**Al** has **N > Z**, its ground state has a $J^{\pi} = 5/2^+$. The calculated excitation energies are compared to the experimental data [14] in Table III. 3. A confrontation of the energy spectrum of ^{27}**Al** to its mirror one of ^{27}**Si** is indispensible, in an attempt to determine the ambiguous states. Note that the **PSDPF** is a Coulomb free and isospin independent interaction, and gives thus the same results for mirror nuclei. Similarly to ^{26}**Al**, **ΔE** denotes the energy difference between theory and experiment, i.e. **ΔE = Eth – Eexp**, and has the same interpretations as in ^{26}**Al** for **ΔE > 400 MeV and ΔE < – 400 MeV**. In the last column, we present the energy difference between the two mirrors ^{27}**Al** and ^{27}**Si**.

From this comparison, we can extract the following comments:

1. There is a one to one correspondence states between theory and experiment for the both mirror ^{27}**Al** and ^{27}**Si**.
2. Same remarks can be seen for the positive- and negative- parity states as in ^{26}**Al**.
3. The comparison of the calculated spectrum to the two mirror spectra permitted us to confirm the unconfirmed J^{π} and to assign the states with uncertain J^{π}. We could also propose J^{π} assignments for states with unknown J^{π}.

Table III. 3: Comparison experimental [14] versus theory of the energy spectra of ^{27}**Al**.

J^{π}_{exp}	^{27}Al	J^{π}_{i}	Eth	ΔE	^{27}Si	ΔE	ΔE=EAl-ESi
$5/2^{+}$	0	$5/2^{+}_{1}$	0	0	0	0	0
$1/2^{+}$	0.844	$1/2^{+}_{1}$	0.897	0.053	0.781	0.116	0.058
$3/2^{+}$	1.015	$3/2^{+}_{1}$	0.987	-0.028	0.957	0.03	0.058
$(7/2^{+})$	2.212	$7/2^{+}_{1}$	2.272	0.06	2.164	0.108	0.048
$5/2^{+}$	2.735	$5/2^{+}_{2}$	2.617	-0.118	2.648	-0.031	0.087
$3/2^{+}$	2.982	$3/2^{+}_{2}$	2.982	0	2.866	0.116	0.116
$(9/2^{+})$	3.004	$9/2^{+}_{1}$	3.022	0.018	2.910	0.112	0.094
$1/2^{+}$	3.680	$1/2^{+}_{2}$	3.95	0.27	3.540	0.41	0.14
$3/2^{+}$	3.957	$3/2^{+}_{3}$	4.081	0.124	3.804	0.277	0.153
$1/2^{-}$	4.055	$1/2^{-}_{1}$	3.019	-1.036	4.138	-1.119	-0.083
$5/2^{+}$	4.410	$5/2^{+}_{3}$	4.391	-0.019	4.289	0.102	0.121
$(11/2^{+})$	4.510	$11/2^{+}_{1}$	4.627	0.117	4.447	0.18	0.063
$(7/2^{+})$	4.58	$7/2^{+}_{2}$	4.848	0.268	4.475	0.373	0.105
$5/2^{+}$	4.812	$5/2^{+}_{4}$	4.768	-0.044	4.704	0.064	0.108
$3/2^{-}$	5.156	$3/2^{-}_{1}$	3.872	-1.284	5.227	-1.355	-0.071
$5/2^{+}$	5.248	$5/2^{+}_{5}$	5.38	0.132	5.062	0.318	0.186
$(9/2^{+})$	5.420	$9/2^{+}_{2}$	5.309	-0.111	5.317	-0.008	0.103
7/2	5.433	$7/2^{+}_{3}$	5.571	0.138	5.262	0.309	0.171
$5/2^{-}$	5.438	$5/2^{-}_{1}$	4.76	-0.678	5.208	-0.632	0.046
$11/2^{+}$	5.500	$11/2^{+}_{2}$	5.552	0.052	5.283	0.269	0.217
5/2	5.551	$5/2^{+}_{6}$	5.672	0.121	5.392	0.28	0.159
$9/2^{+}$	5.667	$9/2^{+}_{3}$	6.028	0.361	5.547	0.481	0.12
$1/2^{+}$	5.752	$1/2^{+}_{3}$	5.971	0.219	5.497	0.474	0.255
$3/2^{-}$	5.827	$3/2^{-}_{2}$	6.144	0.317			
(7/2)	5.960	$7/2^{+}_{4}$	6.034	0.074	5.580	0.454	0.38
3/2	6.081	$3/2^{+}_{4}$	6.078	-0.003	5.613	0.465	0.468
5/2	6.116	$5/2^{+}_{7}$	6.498	0.382	6.323	0.175	-0.207
$3/2^{-}$	6.158	$3/2^{-}_{3}$	7.281	1.123	7.436	-0.155	-1.278
$(7/2^{+})$	6.285	$\mathbf{7/2^{-}_{1}}$	6.254	-0.031	5.897	0.357	0.388
5/2	6.463	$5/2^{+}_{8}$	6.708	0.245	6.572	0.136	-0.109
$(7/2)^{-}$	6.477	$7/2^{-}_{2}$	6.442	-0.035	6.059	0.383	0.418
9/2	6.512	$9/2^{+}_{4}$	6.648	0.136	6.457	0.191	0.055
$7/2^{+}$	6.533	$7/2^{+}_{5}$	6.246	-0.287	5.783	0.463	0.75
$3/2^{-}$	6.605	$3/2^{-}_{4}$	7.688	1.083	7.493	0.195	-0.888
$5/2^{-}$	6.651	$5/2^{-}_{2}$	6.639	-0.012	6.346	0.293	0.305
$9/2^{+}$	6.713	$9/2^{+}_{5}$	6.882	0.169	7.006	-0.124	-0.293
5/2	6.765	$5/2^{+}_{9}$	6.933	0.168	6.780	0.153	-0.015
(3/2)	6.776	$3/2^{+}_{5}$	6.411	-0.365	6.028	0.383	0.748
$1/2^{+}$	6.814	$1/2^{+}_{4}$	6.995	0.181	6.626	0.369	0.188

$(3/2^+, 7/2^+)$	6.821	$7/2^+_6$	6.667	-0.154	6.513	0.154	0.308
$11/2^+$	6.948	$11/2^+_3$	7.399	0.451	7.239	0.16	-0.291
(5/2 TO 9/2)	6.993	$5/2^-_3$	7.017	0.024	7.260	-0.243	-0.267
$(1/2, 5/2)^-$	6.996	$1/2^-_2$	6.77	-0.226	6.587	0.183	0.409
$1/2^+$	7.071	$1/2^+_5$	7.003	-0.068	6.715	0.288	0.356
$9/2^+$	7.174	$9/2^+_6$	7.136	-0.038	7.428	-0.292	-0.254
$9/2^-$	7.227	$9/2^-_1$	7.259	0.032	7.059	0.2	0.168
$(1/2^+$ TO $5/2^+)$	7.280	$1/2^+_6$	7.131	-0.149	7.276	-0.145	0.004
$(9/2, 11/2, 13/2)^+$	7.289	$13/2^+_1$	6.821	-0.468	7.134	-0.313	0.155
$11/2^+$	7.400	$11/2^+_4$	7.791	0.391	7.652	0.139	-0.252
$7/2^+$	7.413	$7/2^+_7$	7.011	-0.402	7.080	-0.069	0.333
$(9/2^+, 13/2^+)$	7.443	$13/2^+_2$	7.427	-0.016	7.223	0.204	0.22
$7/2^-$	7.477	$7/2^-_3$	7.412	-0.065	7.341	0.071	0.136
$(3/2^+, 5/2^+)$	7.550	$3/2^+_6$	7.054	-0.496	7.324	-0.27	0.226
$5/2^+$	7.578	$5/2^+_{10}$	7.666	0.088	7.469	0.197	0.109
$(7/2^+$ TO $11/2^+)$	7.660	$7/2^+_8$	7.327	-0.333	7.590	-0.263	0.07
$(3/2^+, 5/2^+)$	7.677	$3/2^+_7$	7.382	-0.295	7.383	-0.001	0.294
$(7/2, 9/2^+)$	7.679	$7/2^+_9$	7.446	-0.233	7.795	-0.349	-0.116
5/2	7.721	$5/2^-_4$	7.345	-0.376	7.694	-0.349	0.027
(3/2, 5/2, 7/2)	7.798	$5/2^+_{11}$	7.749	-0.049	7.532	0.217	0.266
$(7/2^+, 9/2^+)$	7.806	$9/2^+_7$	7.48	-0.326	7.739	-0.259	0.067
$3/2^+$	7.858	$3/2^+_8$	7.798	-0.06	7.557	0.241	0.301
$(5/2^-, 7/2^-)$	7.900	$7/2^-_4$	7.844	-0.056	7.705	0.139	0.195
	7.935	$1/2^-_3$	7.918	-0.017	7.838	0.08	0.097
$(9/2^+, 11/2^+)$	7.948	$9/2^-_2$	7.604	-0.344	7.832	-0.228	0.116
9/2	7.997	$9/2^-_3$	7.866	-0.131	8.156	-0.29	-0.159
7/2	8.037	$7/2^+_{10}$	7.938	-0.099	8.224	-0.286	-0.187
$(5/2^+$ TO $9/2^+)$	8.043	$9/2^+_8$	7.929	-0.114	8.032	-0.103	0.011
$(3/2^+, 5/2^+)$	8.065	$3/2^+_9$	7.912	-0.153	7.900	0.012	0.165
5/2	8.097	$5/2^-_5$	7.907	-0.19	8.200	-0.293	-0.103
$1/2^+$	8.130	$1/2^+_7$	8.158	0.028	8.327	-0.169	-0.197
5/2	8.136	$5/2^+_{12}$	8.098	-0.038	7.967	0.131	0.169
$3/2^-$	8.182	$3/2^-_5$	7.973	-0.209	8.184	-0.211	-0.002
(5/2, 9/2)	8.287	$9/2^+_9$	8.292	0.005	8.287	0.005	0
$(3/2, 5/2)^+$	8.324	$3/2^+_{10}$	7.952	-0.372	7.909	0.043	0.415
	8.361	$3/2^+_{11}$	8.01	-0.351	8.175	-0.165	0.186
$(3/2, 5/2)^+$	8.376	$5/2^+_{13}$	8.261	-0.115	8.356	-0.095	0.02
11/2	8.396	$11/2^-_1$	8.064	-0.332	8.167	-0.103	0.229

	8.408	$11/2^-_2$	8.142	-0.266	8.299	-0.157	0.109
$(3/2, 5/2)^+$	8.421	$3/2^+_{12}$	8.428	0.007	8.450	-0.022	-0.029
7/2	8.442	$7/2^+_{11}$	7.991	-0.451	8.345	-0.354	0.097
$5/2^+$	8.490	$5/2^+_{14}$	8.479	-0.011			
$(1/2, 3/2, 5/2, 7/2)^+$	8.521	$7/2^+_{12}$	8.633	0.112	8.523	0.10966	-0.002
5/2	8.537	$5/2^-_6$	8.419	-0.118	8.376	0.043	0.161
3/2	8.553	$3/2^+_{13}$	8.691	0.138			
7/2	8.586	$7/2^-_5$	8.479	-0.107	8.208	0.271	0.378
$(1/2, 3/2)^-$	8.598	$1/2^-_4$	8.056	-0.542	8.139	-0.083	0.459
$(7/2, 9/2^+)$	8.675	$7/2^+_{13}$	8.65	-0.025	8.669	-0.01902	0.006
(9/2, 11/2, 13/2)	8.693	$11/2^+_5$	8.472	-0.221			
	8.709	$9/2^+_{10}$	8.502	-0.207	8.486	0.01558	0.223
$1/2^+$	8.717	$1/2^+_8$	8.669	-0.048	8.450	0.21907	0.267
$(5/2, 7/2)^-$	8.732	$7/2^-_6$	8.64	-0.092			
5/2	8.754	$5/2^-_7$	8.967	0.213			
$(5/2^+)$	8.774	$5/2^+_{15}$	8.753	-0.021	8.776	-0.02303	-0.002
	8.804	$11/2^+_6$	8.89	0.086			
	8.825	$9/2^-_4$	8.682	-0.143	8.822	-0.1404	0.003
	8.861	$11/2^-_3$	8.702	-0.159	8.864	-0.16176	-0.003
$(5/2^+)$	8.897	$5/2^+_{16}$	8.859	-0.038	8.872	-0.01254	0.025
	8.905	$9/2^-_5$	8.801	-0.104			
$(1/2, 3/2)^-$	8.909	$1/2^-_5$	8.607	-0.302			
$(5/2, 9/2^+)$	8.952	$9/2^+_{11}$	8.852	-0.1	8.931	-0.07869	0.021
$(3/2^-)$	8.963	$3/2^-_6$	8.249	-0.714	8.184	0.065	0.779
	9.001	$13/2^-_1$	8.977	-0.024			
$(7/2^-)$	9.051	$7/2^-_7$	8.912	-0.139			
$(5/2^+)$	9.052	$5/2^+_{17}$	8.966	-0.086			
	9.058	$11/2^+_7$	8.975	-0.083	9.066	-0.09053	-0.008
$1/2^+$	9.080	$1/2^+_9$	8.906	-0.174	9.074	-0.16824	0.006
(3/2)	9.190	$3/2^+_{14}$	8.87	-0.32			
$(3/2^-)$	9.216	$3/2^-_7$	8.668	-0.548	9.215	-0.54679	0.001
$(1/2^+)$	9.236	$1/2^-_6$	8.921	-0.315			
(5/2)	9.240	$5/2^-_8$	9.094	-0.146			
$(1/2^+, 3/2)$	9.272	$3/2^+_{15}$	9.187	-0.085	9.227	-0.04038	0.001
$(5/2^-, 7/2)$	9.274	$7/2^+_{14}$	8.982	-0.292			
$(3/2^-)$	9.277	$3/2^-_8$	9.009	-0.268			
	9.299	$9/2^-_6$	8.995	-0.304			
$(5/2^+)$	9.308	$5/2^+_{18}$	9.175	-0.133	9.308	-0.13258	0
	9.322	$9/2^+_{12}$	9.177	-0.145			
	9.359	$1/2^-_7$	9.221	-0.138			
	9.371	$13/2^+_3$	9.186	-0.185			
$(3/2^+)$	9.390	$3/2^+_{16}$	9.413	0.023			

$(1/2^+)$	9.401	$1/2^+_{10}$	9.039	-0.362	9.409	-0.36957	-0.008
	9.427	$7/2^+_{15}$	9.014	-0.413	9.428	-0.41361	-0.001
(7/2)	9.474	$7/2^+_{16}$	9.147	-0.327	9.477	-0.32962	-0.003
	9.488	$9/2^-_{7}$	9.268	-0.22			
	9.502	$7/2^-_{8}$	9.244	-0.258			
(5/2)	9.512	$5/2^-_{9}$	9.386	-0.126			
	9.530	$7/2^-_{9}$	9.381	-0.149			
	9.552	$11/2^-_{4}$	9.44	-0.112	9.547	-0.10693	0.005
	9.599	$9/2^+_{13}$	9.44	-0.159	9.576	-0.13574	0.023
$(3/2^-)$	9.601	$3/2^-_{9}$	9.423	-0.178			
	9.619	$9/2^-_{8}$	9.567	-0.052			
$(1/2^-)$	9.629	$1/2^-_{8}$	9.479	-0.15			
$(5/2^+)$	9.635	$5/2^+_{19}$	9.353	-0.282			
	9.658	$7/2^-_{10}$	9.538	-0.12	9.655	-0.11684	0.004
$(5/2^+)$	9.665	$5/2^+_{20}$	9.483	-0.182			
$(1/2^-)$	9.665	$1/2^-_{9}$	9.896	0.231			
	9.692	$15/2^+_{1}$	9.518	-0.174			
$(3/2^+)$	9.716	$3/2^+_{17}$	9.624	-0.092	9.715	-0.09081	0.001
	9.742	$11/2^+_{8}$	9.644	-0.098			
$(5/2^+)$	9.763	$5/2^+_{21}$	9.802	0.039			
$(7/2^+)$	9.796	$7/2^+_{17}$	9.473	-0.323	9.791	0.03817	-0.001
$(3/2^+)$	9.822	$1/2^-_{10}$	9.578	-0.244			
$(1/2^-)$	9.834	$1/2^-_{10}$	10.055	0.221	9.834	0.22139	0
(5/2)	9.840	$5/2^-_{10}$	9.615	-0.225			
$(1/2^+)$	9.847	$1/2^+_{11}$	9.555	-0.292	9.856	-0.30084	-0.009
	9.867	$13/2^+_{4}$	9.673	-0.194			
	9.883	$11/2^-_{5}$	9.685	-0.198			
	9.893	$11/2^+_{9}$	9.693	-0.2	9.895	-0.20227	-0.002
$(3/2^-)$	9.923	$1/2^-_{11}$	9.855	-0.068	9.934	-0.07926	-0.011
$(1/2^-)$	9.930	$1/2^+_{12}$	9.821	-0.109			
(7/2)	9.941	$7/2^+_{18}$	9.75	-0.191			
	9.953	$9/2^-_{9}$	9.685	-0.268			
(3/2)	9.956	$3/2^+_{18}$	9.856	-0.1			
$(5/2^-)$	9.960	$5/2^-_{11}$	9.841	-0.119			
$(5/2^+)$	9.963	$5/2^+_{22}$	10.013	0.05			
$(7/2, 5/2)^+$	9.977	$7/2^+_{19}$	9.868	-0.109			
$(7/2^-)$	9.991	$7/2^+_{20}$	10.079	0.088			
(5/2)	10.000	$5/2^-_{12}$	10.147	0.147			

As was done for **^{26}Al**, we present the rmsd values in Table III. 4. The energy difference, **ΔE**, for the first **0ħω** and **1ħω** states are shown in Figure III. 2, here the **1ħω** states are better reproduced than those in **^{26}Al**.

Table III. 4: The **rmsd** values (in keV) in ^{27}**Al**.

States	All states	0ħω states	1ħω states
rmsd	287	210	379

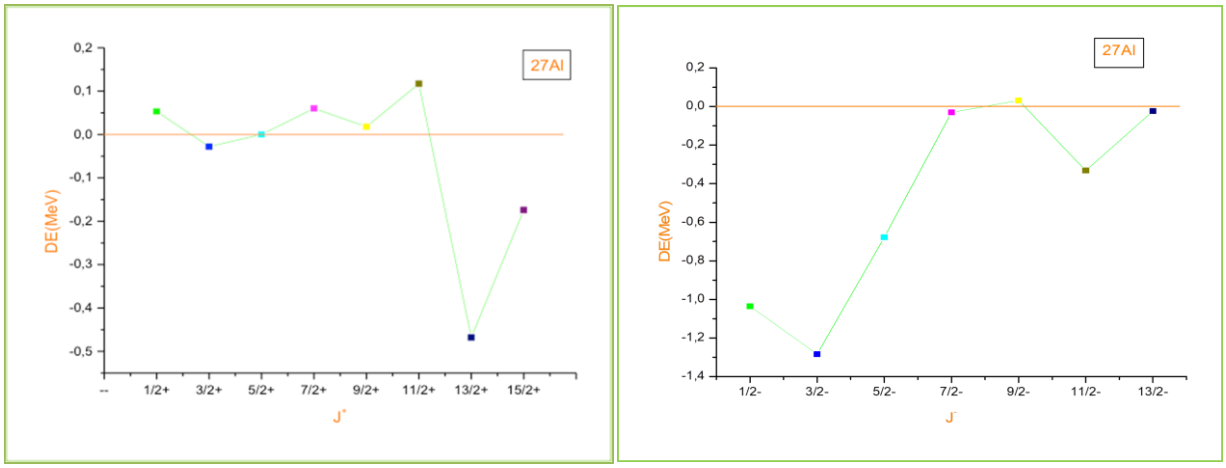

Figure III. 2: Energy difference, **ΔE**, for the first $\mathbf{J}^{+}$ and $\mathbf{J}^{-}$ states in ^{27}**Al**.

II.2. Half-lives in ^{27}Al

We calculated, using the **PSDPF** interaction, the electromagnetic properties of the first observed states in the mirrors ^{27}**Al** and ^{27}**Si** that have known **half-lives**. The comparison of the obtained **half-lives** to the experimental ones [14] is shown in Table III. 5. We can see the good agreement between theory and experiment. The entire calculated **half-lives** have the same order of magnitude as experimental ones.

Table III. 5: Comparison experimental [14] versus calculated **half-lives** in ^{27}**Al** and ^{27}**Si**.

J^{π}_i	$T_{1/2}^{(exp)}$ ^{27}Al	$T_{1/2}^{(the)}$ ^{27}Al	$T_{1/2}^{(exp)}$ ^{27}Si	$T_{1/2}^{(the)}$ ^{27}Si
$1/2^+_1$	35 ps	38 ps	35 ps	24 ps
$3/2^+_1$	1.49 ps	7.07 ps	1.20 ps	5.07 ps
$7/2^+_1$	26.6 fs	28.4 fs	44 fs	42 fs
$5/2^+_2$	8.9 fs	8.7 fs	17 fs 15 fs[a]	12 fs
$3/2^+_2$	3.90 fs	2.9 fs	< 3 fs	5 fs
$9/2^+_1$	59 fs	52 fs	52 fs	35 fs
$1/2^+_2$	5.4 fs	5.1 fs	<5 fs 10 fs[a]	5 fs
$3/2^+_3$	2.5 fs	3.2 fs	<7 fs <1 fs[a]	4 fs
$1/2^-_1$	7.3 fs	128 fs	6 fs 8 fs[a]	95 fs
$5/2^+_3$	1.2 fs	0.7 fs	3.5 fs 4 fs[a]	1.0 fs
$11/2^+_1$	222 fs	241 fs	390 fs	265 fs
$7/2^+_2$	5.3 fs	5.3 fs	<7 fs 11 fs[a]	8 fs
$5/2^+_4$	1.5 fs	14.4 fs	<5 fs 7 fs[a]	13 fs
$3/2^-_1$	2.4 fs	1.0 fs		1 fs
$5/2^+_5$	<4 fs	1 fs	21 fs	1 fs
$9/2^+_2$	<14 fs	3.4 fs	<31 fs 7 fs[a]	5 fs
$7/2^+_3$	7 fs	3 fs	10 fs[a]	4 fs
$5/2^-_1$	6 fs	3 fs	<35 fs	117 fs
$11/2^+_2$	<7 fs	11 fs	17 fs 9 fs[a]	13 fs
$5/2^+_6$	2.6 fs	6.4 fs	<31 fs <30 fs[a]	7 fs
$9/2^+_3$	11 fs	18 fs	14 fs[a]	30 fs
$1/2^+_3$	<10 fs	3 fs	<10 fs 8 fs[a]	4 fs

(a) Values taken from Ref. [60]

In this chapter, we used the **PSDPF** interaction to describe the complete energy spectra of both positive- and negative- parity states in ^{26}**Al** and ^{27}**Al**. The comparison of our results to the observed excitation energies and half-lives shows a satisfactory agreement. **PSDPF** interaction allowed us to confirm the uncertain states (levels with uncertain $\mathbf{J^{\pi}}$) and to predict $\mathbf{J^{\pi}}$ assignments for the unidentified ones (states with unknown $\mathbf{J^{\pi}}$).

Conclusion

Conclusion

Experimental and theoretical studies in nuclear physics played a significant role in the development of the 20th century physics. Among of the theoretical work, we employed the shell model framework using the **PSDPF** interaction to study the spectroscopic properties of both ^{26}**Al** and ^{27}**Al** isotopes.

The main aim of our work was the calculation of the excitation energy spectra, and electromagnetic transitions, of ^{26}**Al** and ^{27}**Al**, in order to determine the $\mathbf{J^{\pi}}$ of the ambiguous states and to predict spins and/or parities assignments for the unknown states.

The obtained results show a good agreement theory versus experiment for all the studied spectroscopic properties of the ^{26}**Al** and ^{27}**Al**. In order to determine the $\mathbf{J^{\pi}}$ of the uncertain and unknown levels in the ^{26}**Al**, we used its **T=1** isobaric mass doublet, ^{26}**Mg** and ^{26}**Si**. Similarly, we used the mirror nucleus ^{27}**Si** for the ^{27}**Al**.

In conclusion, this study gives more credit to the **PSDPF** interaction in reproducing the spectroscopic properties of nuclei in the middle of the **sd** shell, which could not be included in its fitting procedure.

Bibliography

Bibliography

[1] M. Bouhelal, PhD Thesis, under joint supervision of University of Batna, Algeria and University of Strasbourg, France (2010).

[2] P. J. Brussaard, P. W. M. Glaudemans, "Shell–Model Applications in Nuclear Spectroscopy", North–Holland, (1977).

[3] M. G. Mayer, Phys. Rev. 75, 1969 (1949).

[4] O. Haxel, J. H. D. Jensen and H. E. Suess, Phys. Rev.75, 1766 (1949).

[5] R. R. Whitehead, A. Watt, B. J. Cole, I. Morrison, Adv. Nucl. Phys. 9, 123 (1977).

[6] E. Caurier, F. Nowacki, Acta Phys. Pol. B 30, 705 (1999).

[7] A. Schmidt et al, Phys. Rev. C 62, 044319 (2000).

[8] T. Mizusaki, RIKEN Accelerator Progress Report Vol. 33, 15 (2000).

[9] E. W. Ormand, C. W. Johnson, REDSTICK code, 2002.

[10] D. Zwarts, Comp, Phys, Comm. 38, 365 (1985).

[11] B. A. Brown et al., MSU–NSCL Report No. 524 (1985).

[12] A. Novoselsky, M. Vallières, Drexel University Shell–Model Code DUPSM (1997).

[13] E. Caurier et al., Phys. Rev. C 59, 2033 (1999).

[14] http://www.nndc.bnl.gov/nudat2 .

[15] B. A. Brown, B. H. Wildenthal, Nucl. Phys, A474, 290, (1987).

[16] B. H. Wildenthal, Prog. Part. Nucl. Phys. 11, 5 (1984).

[17] B. A. Brown, W. A. Richter, Phys. Rev., C 74, 034315 (2006).

[18] M. Bouhelal et al., Nucl. Phys. A 864, 113 (2011), and references therein.

[19] M. Bouhelal, F. Haas, E. Caurier, F. Nowacki, AIP Conf. Proc.1165, 61 (2009).

[20] M. Bouhelal, F. Haas, E. Caurier, F. Nowacki, Journal of Physics: Conference Series 580, 012025 (2015).

[21] M. Bouhelal, and F. Haas, Eur. Phys. J. Plus 131, 226 (2016).

[22] M. Bouhelal, M. Labidi, F. Haas, Few- Body Syst, Volume 58, Issue 2, article id.58, 4 pp (2017).

[23] M. Bouhelal, N. Azzeddine, N. Chorfi, F. Haas, Nuclear Theory, Vol. 37, 204 (2018), Heron Press, Sofia.

[24] M. Labidi, Master's Thesis, University of Tebessa, Algeria (2013).

[25] N. Chorfi, N. Azzeddine, Master's Thesis, University of Tebessa, Algeria (2017).

[26] M. Bouhelal, F. Haas, E. Caurier, F. Nowacki, AIP Conf. Proc.1491, 38 (2012).

[27] M. Abid, Master's Thesis, University of Tebessa, Algeria (2014).

[28] F. Drar, R. Bouchiba, Master's Thesis, University of Tebessa, Algeria (2017).

[29] H. Mebrek, M. Bouhelal, D. Bahloul, Nuclear Theory Vol. 38, 94 (2019) Heron Press, Sofia.

[30] H. Laidoudi, Master's Thesis, University of Tebessa, Algeria(2019) .

[31] A. Selim, K. Selim, Master's Thesis, University of Tebessa,Algeria(2020) .

[32] O. Ramdane, G. Fassekh, Master's Thesis, University of Tebessa, Algeria (2020).

[33] R. Mecheri, R. Doubia, Master's Thesis, University of Tebessa, Algeria (2021) .

[34] M. R. Haouam, M. Bouhelal, F. Haas, E. Caurier, F. Nowacki, AIP Conf. Proc.1444, 375 (2012).

[35] M. R. Haouam, Master's Thesis, University of Tebessa, Algeria (2011).

[36] M. Bouhelal, F. Haas, E. Caurier, F. Nowacki, PoS (NIC XIII) 074 (2015), 5 pp., Proc. XIII Nuclei in the Cosmos (2014).

[37] M. Bouhelal, N. Saidane, S. Belaid, F. Haas, Can. J. Phys. 96 (7), 774 (2018).

[38] N. Saidane, S. Belaid, Master's Thesis, University of Tebessa, Algeria (2017).

[39] S. Aydin et al., Phys. Rev. C 89, 014310 (2014).

[40] R. Chapman et al., Phys Rev C 93, 044318 (2016).

[41] R. Chapman et al., Phys Rev C 94, 024325 (2016).

[42] B. Fu et al., Phys Rev C 94, 034318 (2016).

[43] S. Aydin et al., Phys Rev C 96, 024315 (2017).

[44] R. Chapman et al., Phys Rev C 92, 044308 (2015).

[45] R. S. Lubna et al., Phys Rev C 97, 044312 (2018).

[46] L. Grocutt, R. Chapman , M. Bouhelal et al ., Phy Rev C 100, 064308 (2019)

[47] Z. M. Wang et al., Phys. Rev. C 81, 064301 (2010).

[48] S. Aydin et al., Phys. Rev. C 86, 024320 (2012).

[49] S. Szilner et al., Phys. Rev. C 87, 054322 (2013).

[50] S. Aydin, et al., Journal of Physics: Conference Series 590, 012036 (2015).

[51] S. Szilner et al., Phys. Rev. C 84, 014325 (2011).

[52] P. Marley et al., Phys. Rev. C 84, 044332 (2011).

[53] D.G. Jenkins, M. Bouhelal, et al., Phys. Rev. C 87, 064301 (2013).

[54] W. A. Richter, S. Mkhize, and B. Alex Brown, Phys. Rev. C 78, 064302 (2008).

[55] M. Bouhelal, M. Labidi, F. Haas, E. Caurier, Phys. Rev. C 96, 044304 (2017).

[56] M. Thoennessen, At. Data Nucl. Data Tables 98, 933 (2012).

[57] M. S. Basunia and A. M. Hurst, Nucl Data sheets 134,1 (2016).

[58] M. S. Basunia, Nucl Data sheets, 112, 1875 (2011).

[59] A. Kankainen et al ., Phys .Lett. B 813, 136033 (2021).

[60] G. Lotay et al., Phys. Rev. C 84, 035802 (2011).